Chapter IV

Results

4.1 Results of Powder Preparation

4.1.1 Result of Density : The density of OX-50 is 2.20 ± 0.02 g/cm^3. The density of rice husk ash is 2.14 ± 0.05 g/cm^3 by measurment.

4.1.2 Result of XRD : Figure 4.1 shows OX-50, ash and classified ash powders which are both amorphous materials (X-rays amorphous).

4.1.3 Results of SEM : OX-50 is illustrated in figure 4.2. It has better dispersion than rice husk ash in figure 4.3 because rice husk ash has agglomeration. The SEM micrographs in figure 4.4 show rice husk ash which was grinded before classifying. Figures 4.4 and 4.5 demonstrates the ability of the classifier device. Figure 4.6 illustrates the rest (the discard) of rice husk ash which did not pass the classifier. This part can be ground again.

4.2 Results of Gel Formation

4.2.1 Role of Conditions : Gel formation conditions are important. If the conditions are not appropriate, a gel will not form.

So, gelation was studied varying factors such as kinds of binder, % of binder, pH control, kinds of solution for mixing, which is illustrated in table 4.1.

4.2.2 Results of XRD : Figure 4.7 shows that the gel, as received are amorphous.

4.2.3 Results of SEM : Figures 4.8 - 4.9 compare the results for different gel preparation routes.

4.3 Results of Drying

4.3.1 Results of Temperature Control : Tables 4.2 - 4.3 describe the effect of temperature on drying. This is also illustrated in figures 4.10 - 4.12. The results for all other temperatures of experimentation can be seen in the annex.

4.3.2 Results of Humidity Control : Table 4.4 shows the results for humidity 0, 30, 50, 70, 90% at 70°C, 90°C. This is also illustrated in figures 4.13, 4.14, 4.15 , and 4.16. The results of all other humidities can be seen in the annex. Beside this, the relationship between log slope (weight loss) and pressure in mm.Hg (see table 4.5) is established. Figure 4.18 shows the relationship between log slope (weight loss) and pressure in mm.Hg at 70°C and 90°C.

4.4 Results of Sintering

4.4.1 Role of Sintering Temperature : The temperature is

important for complete sintering without occurance of a crystalline phase. So, different temperature were studied i.e., 1100, 1150, 1200, 1300, 1350, and 1400°C for OX-50 and 1250, 1300, 1350, 1400, 1450, 1500 °C for rice husk ash. All results of OX-50 are contained in the annex. Table 4.6 shows examples for sintering temperature, which are also shown in figures 4.18 - 4.20. Beyond this, figure 4.21 shows the microstructure of sintered samples. Figure 4.22 shows the times which are appropriate for sintering, figure 4.23 is used to compare results with figures 4.24 - 4.28 on the microstructure of gel homogeneity. Figure 4.23 shows a heterogeneous gel prepared from rice husk ash with NH_4F (no pH control). Figures 4.24 - 4.28 show microstructure after sintering at different temperatures and times. Figures 4.29 - 4.31 show X-ray patterns of amorphous and crystalline phase at different temperatures and times. Then, figure 4.32 concludes the results in a TTT diagram for OX-50 and rice husk ash from data as received.

4.5 Results of Characterization

4.5.1 The Results of Characterization : Table 4.7 shows properties after sintering at different temperatures. Figure 4.33 shows the thermal expansion curves of a standard glass, OX-50 and silica glass of rice husk ash. Table 4.8 shows the different properties of SiO_2. From this table, it becomes obvious that the thermal expansion is a very strict indicator for the nature of silica. Only the vitreous silica has the extremely low thermal expansion. Any crystalline phase that might from (i.e., cristobalite or tridymite) have thermal expansions higher by more than a factor 10.

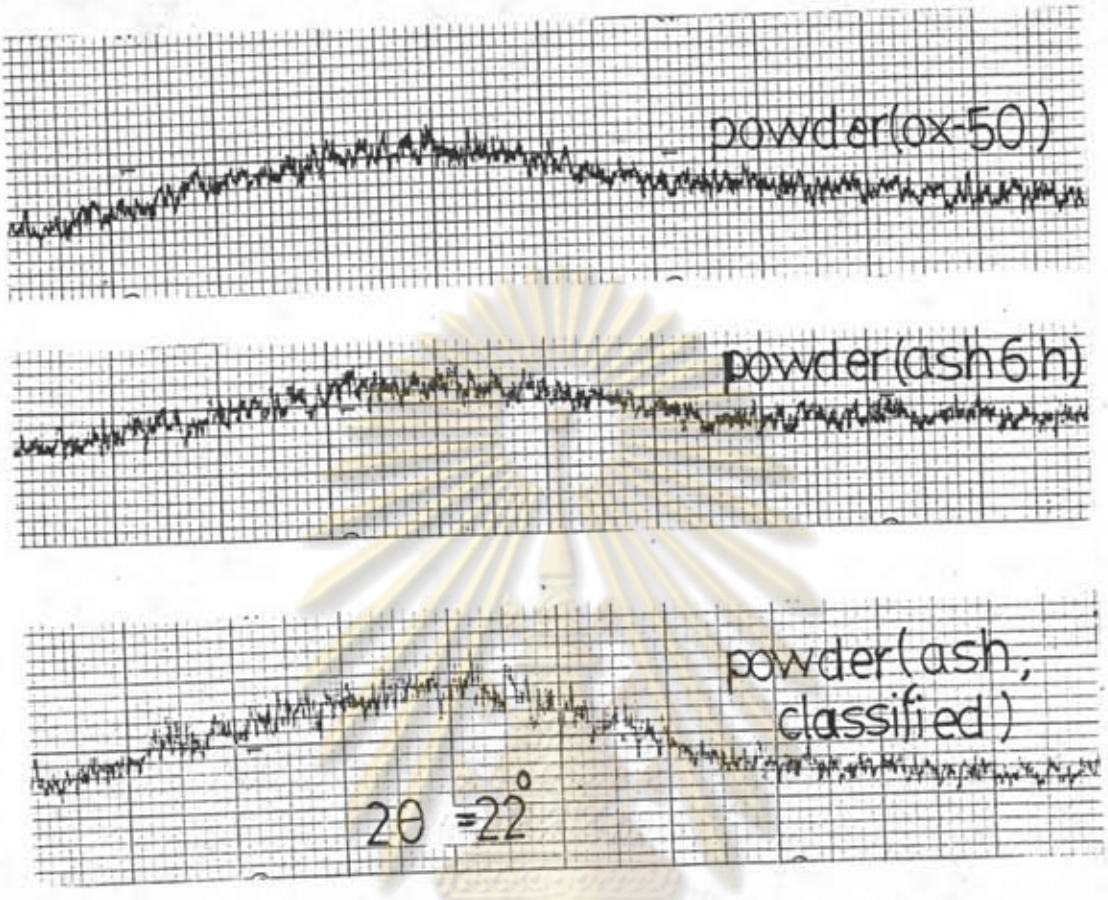

Figure 4.1: X-ray diffraction patterns showing amorphous powder

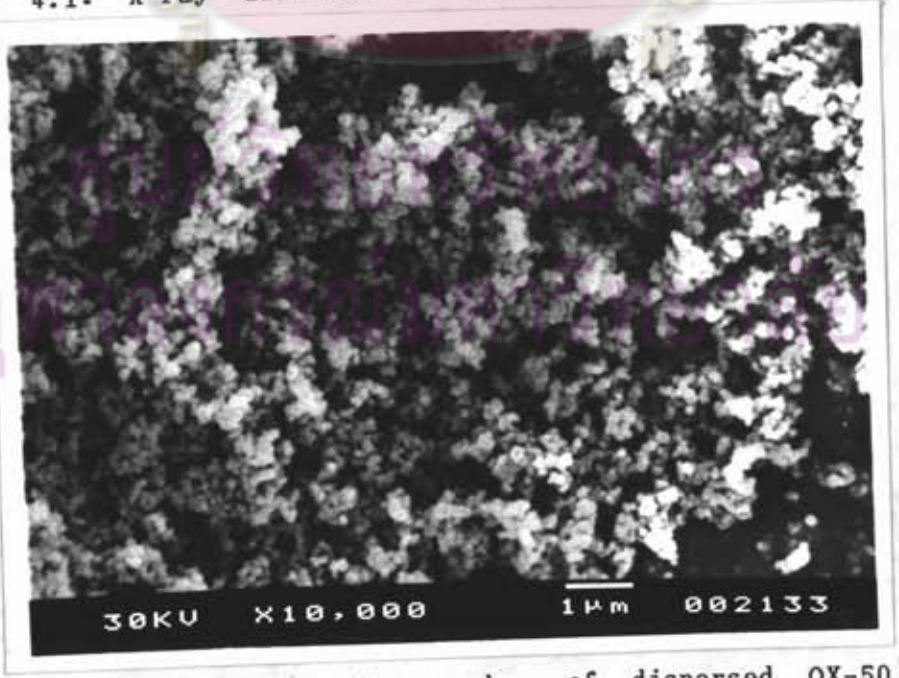

Figure 4.2: SEM micrographs of dispersed OX-50

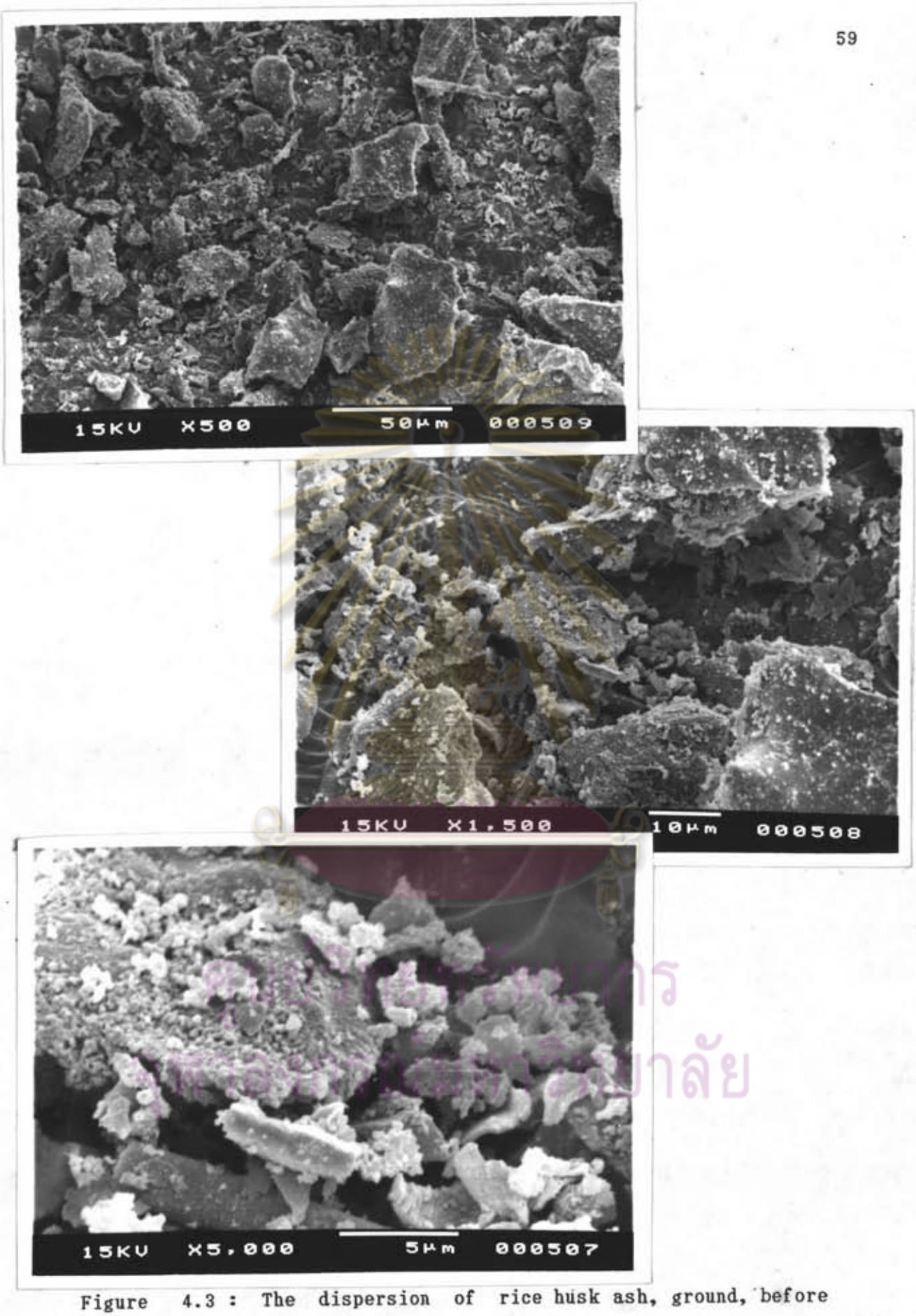

Figure 4.3 : The dispersion of rice husk ash, ground, before passing through the particle classifier

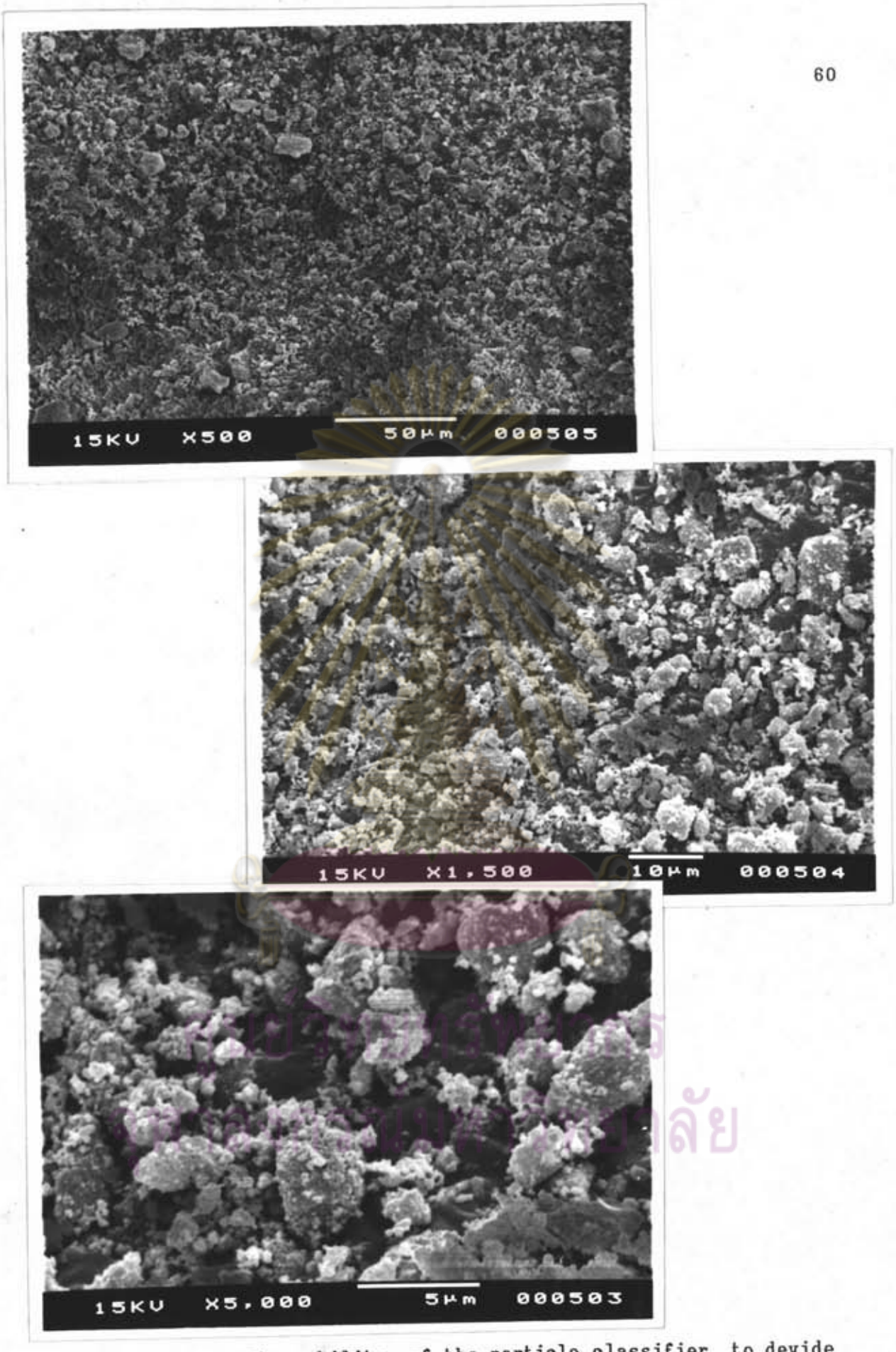

Figure 4.4 : The ability of the particle classifier to devide particle sizes of rice husk ash (low air flow)

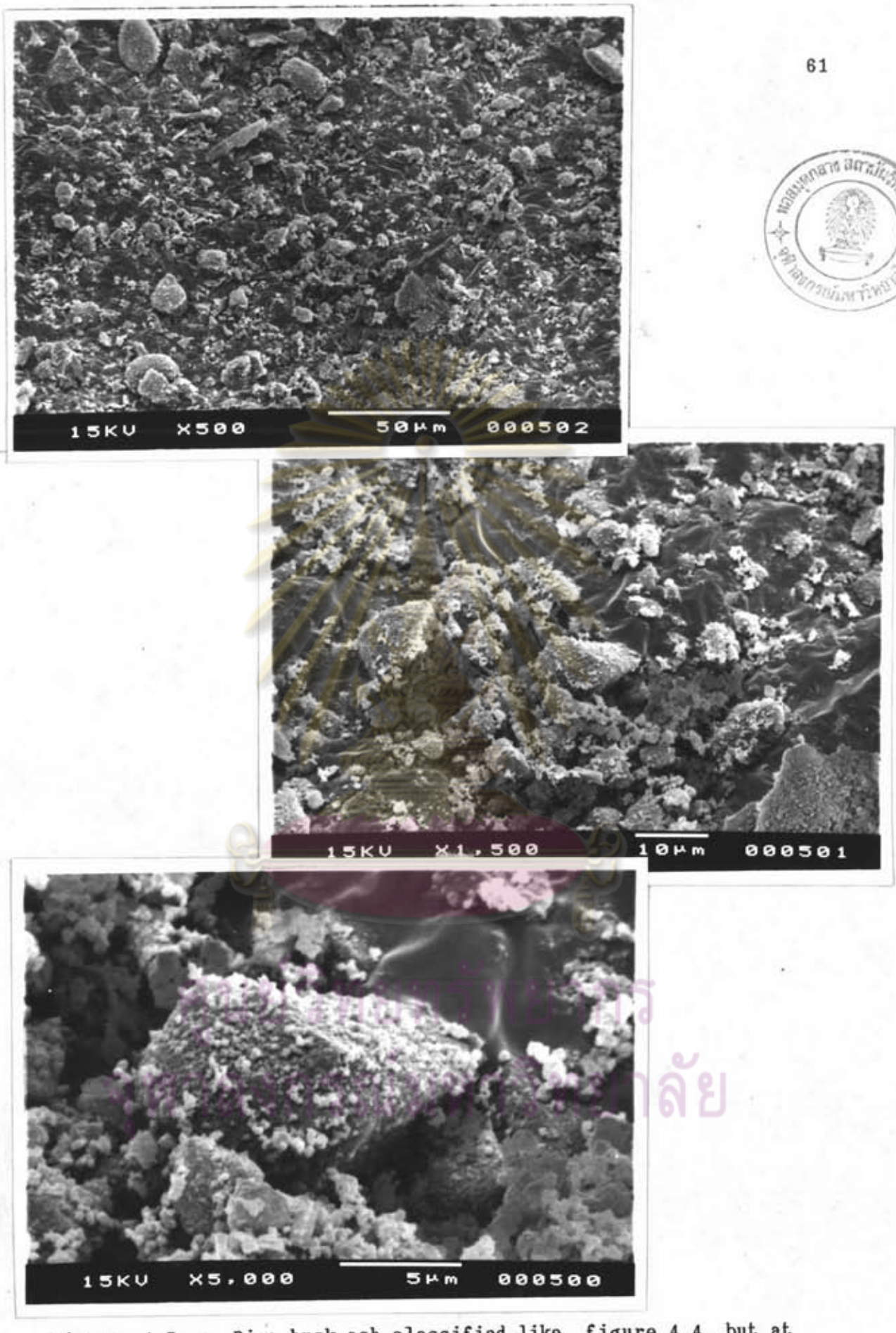

Figure 4.5 : Rice husk ash classified like figure 4.4, but at high air flow

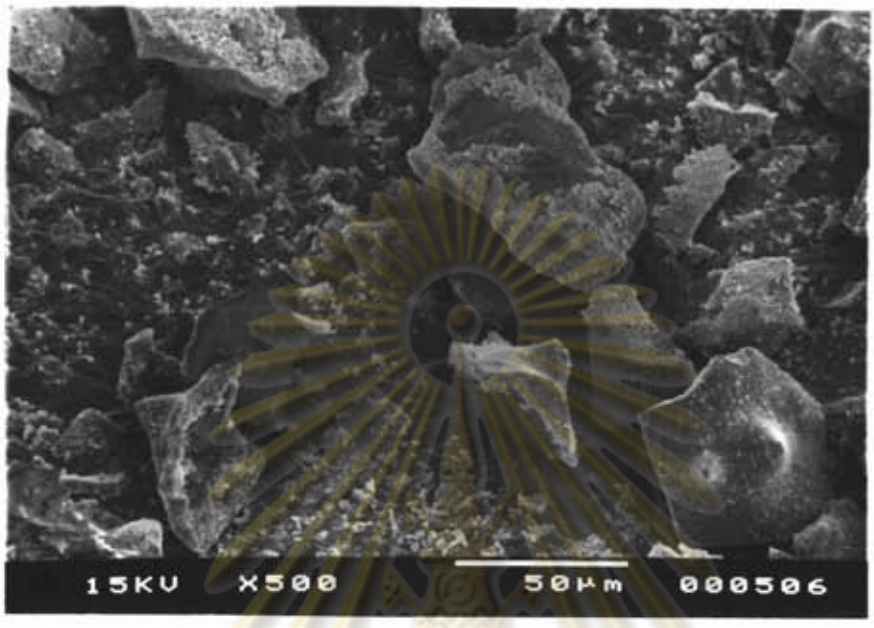

Figure 4.6 : The discard of rice husk ash, which did not pass the classifier

Table 4.1: Conditions for gelation

binder (A200)* wt.% in solution	not adjusting pH			adjusting pH with HCl, NH_4OH		
	H_2O	H_3BO_3	NH_4F	H_2O	H_3BO_3	NH_4F
5		sol	gel		sol	sol <(5 min)--> gel
10	gel	sol	gel	gel <(>10 min)--> sol	sol <(>5 min)--> gel	sol <(5 min)--> gel
20	gel	metagel	gel	gel <(>10 min)--> sol	sol <(>5 min)--> gel	sol <(5 min)--> gel

*) A200 is a pyrogenic silica with a specific surface area of 200 m^2/g.

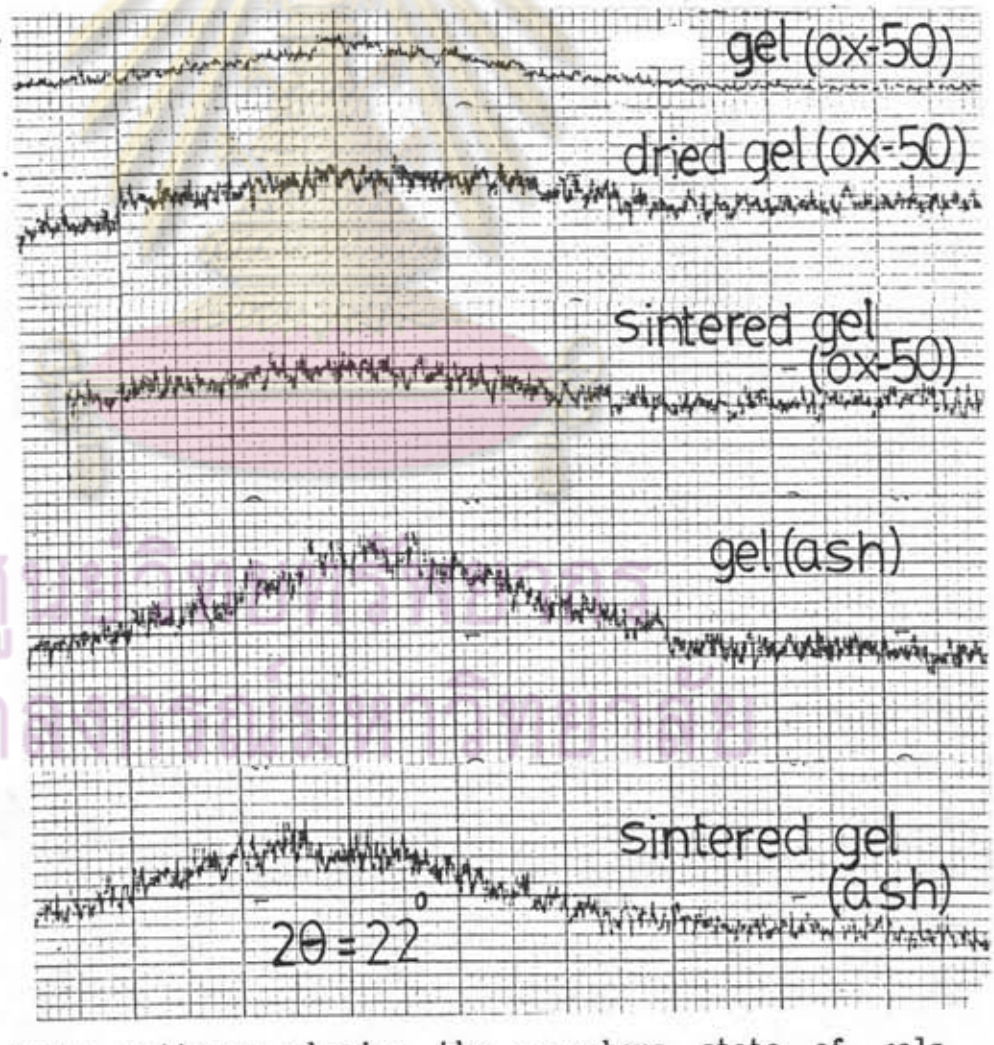

Figure 4.7: X-ray patterns showing the amorphous state of gels and sintered gels

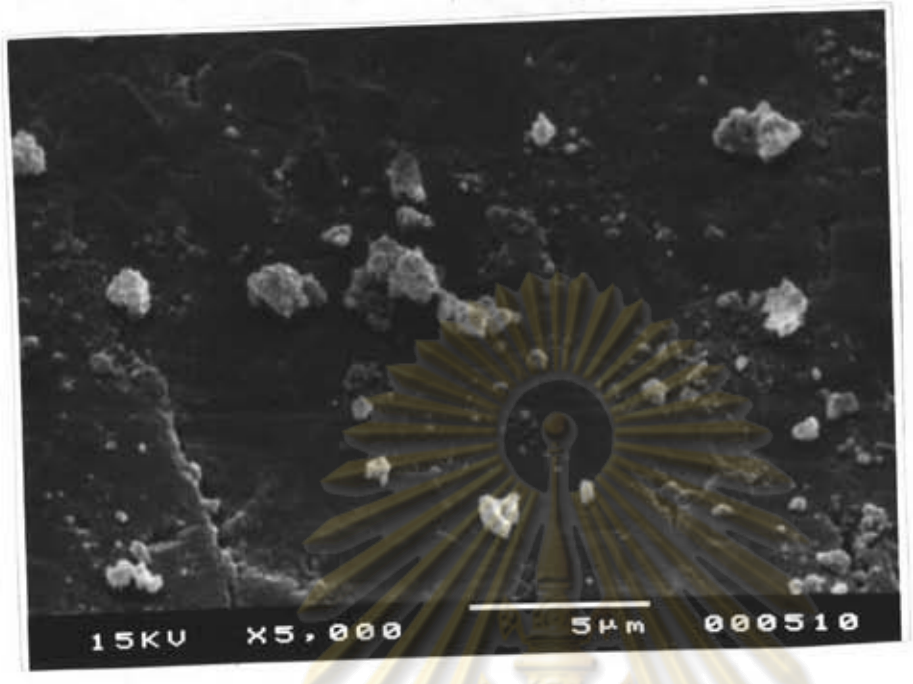

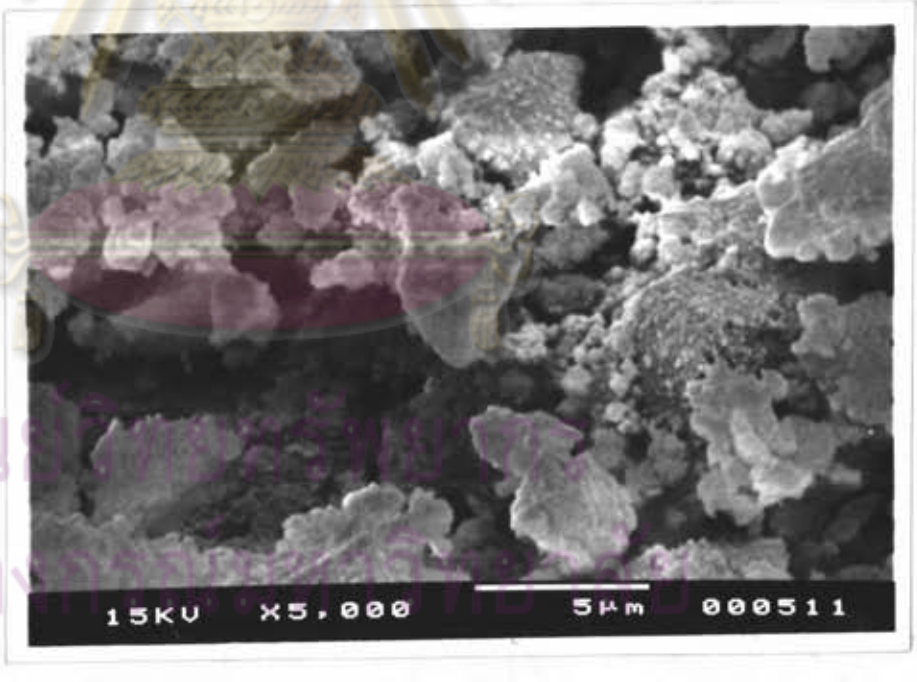

Figure 4.8: SEM micrographs of the microstructure of gels from rice husk ash with NH_4F solution

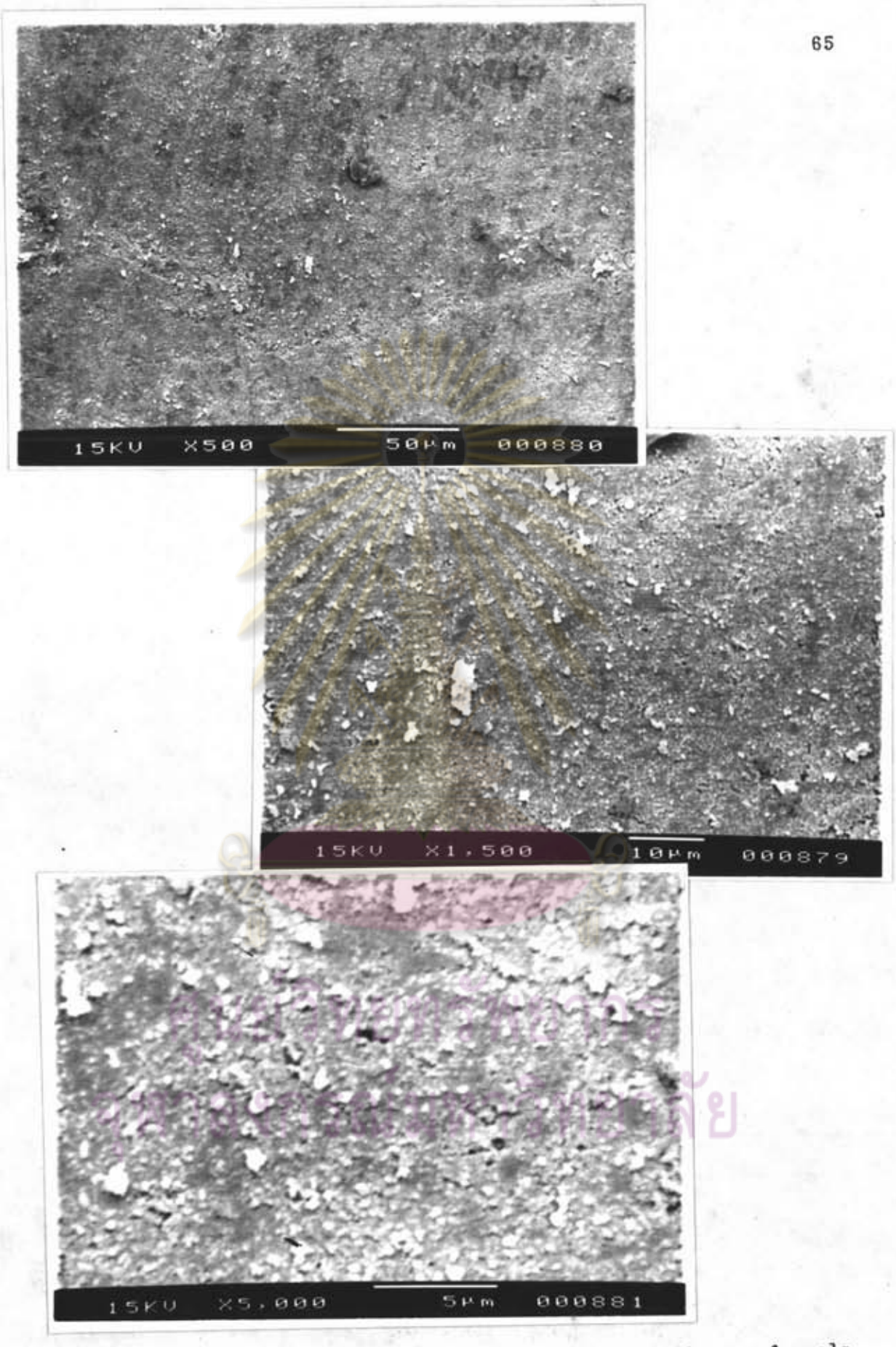

Figure 4.9: SEM micrographs of the microstructure of gels from rice husk ash with H_3BO_3 solution

Table 4.2: The effect of temperature on drying (example 70°C)

time(hour)	% weight loss(avg.)	%shrinkage
0	8.91	100.00
1	18.35	97.32
2	27.83	87.42
3	36.86	78.48
4	45.56	71.62
5	54.01	67.78
6	62.43	68.89
7	70.60	68.89
8	78.50	68.89
9	86.05	68.89
10	92.95	68.89
11	97.39	68.89
12	99.59	68.89
13	99.66	68.89

The slope of weight loss vs. time curve is 8.54 .

The slope of shrinkage vs. time curve is -8.60.

Both of the slopes of weight loss and shrinkage are determined from curves in figure 4.11. The values of slopes at temperature 50, 90, 110, 150, 200, 300 °C are in annex.

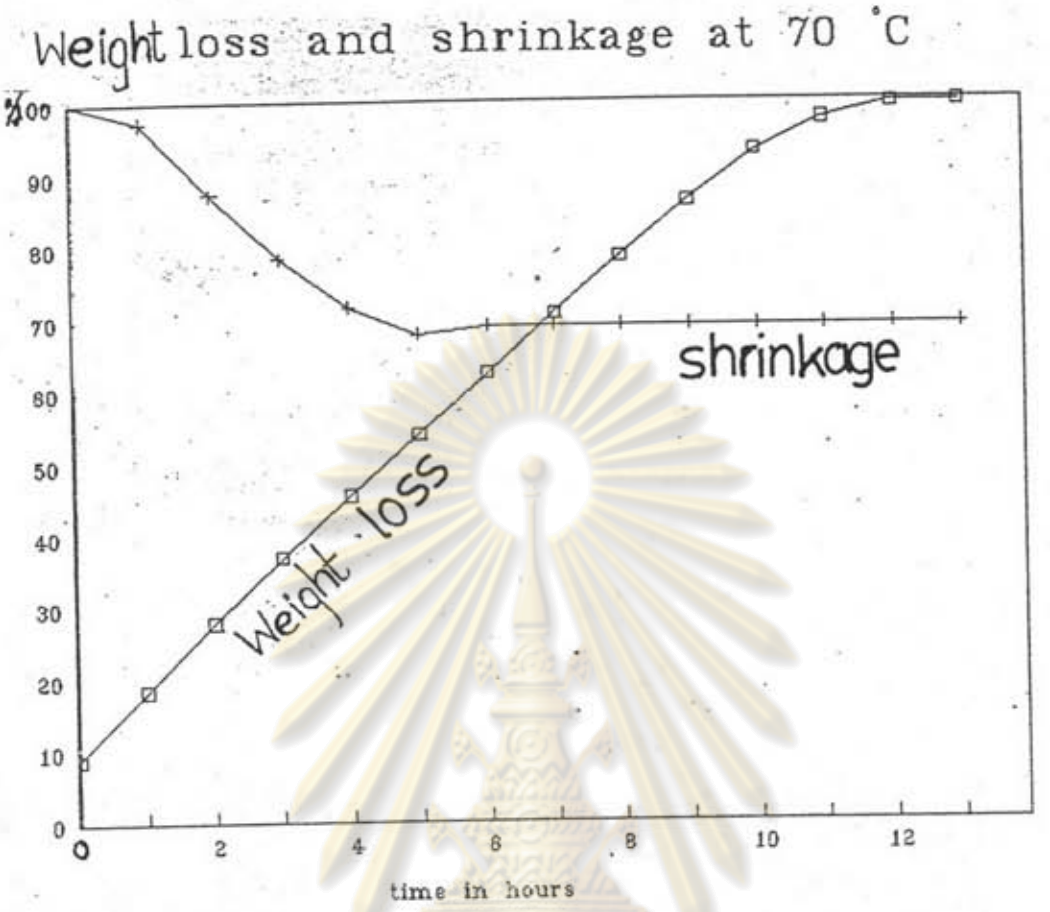

Figure 4.10: Weight loss and shrinkage values of OX-50 at 70°C

Table 4.3: The effect of temperature on drying in Arrhenius equation

Temperature on drying (°C)	1/T in 1000/K	drying rate*	shrinkage rate
50	3.09	4.09	-3.65
70	2.91	8.54	-8.60
90	2.75	16.64	-9.56
110	2.61	20.59	-11.73
150	2.36	38.09	-23.03
200	2.11	71.57	-40.92
300	1.74	306.46	-292.20

*) is the drying rates are determined from the slopes of the weight loss vs. time curves in figure 4.11.

The slope (drying rate) is -1.30 in figure 4.12.

The slope (shrinkage rate) is -1.27 in figure 4.13.

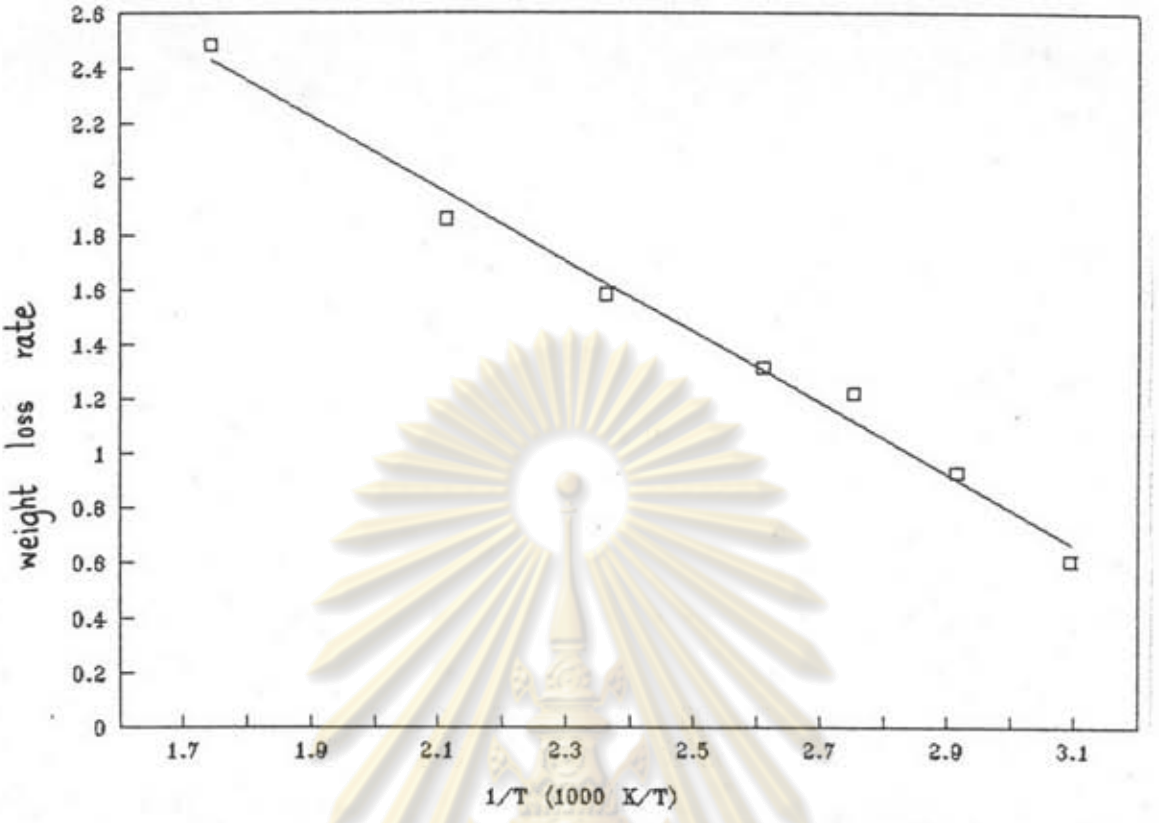

Figure 4.11 : Arrhenius plot of weight loss upon drying

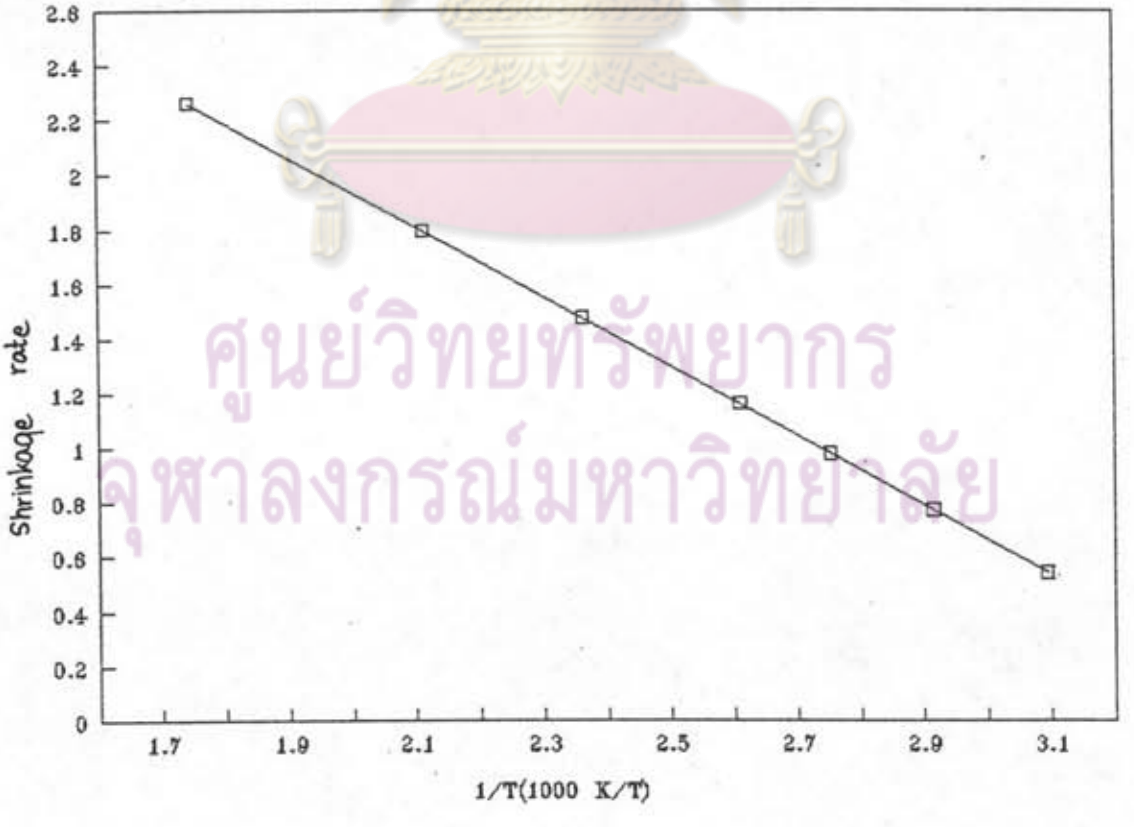

Figure 4.12 : Arrhenius plot of shrinkage upon drying

Table 4.4: Humidity control on drying at 0, 30, 50, 70, 90% ($P^{\circ}_{H_2O}$ = 70°C, 90°C)

% relative humidity	drying rate		shrinkage rate	
	70°C	90°C	70°C	90°C
0	8.04	11.13	-9.65	-11.47
30	7.86	11.13	-9.95	-9.80
50	5.79	10.17	-7.38	-11.00
70	6.26	6.37	-6.72	-6.14
90	3.00	2.37	-3.71	-2.55

Weight loss and shrinkage rates (marked as "slope") at different relative humidities and temperatures.

$P^{\circ}_{H_2O}$ is the pressure of water bath at 70, 90 °C.

The drying and shrinkage rates are determined from curves in figure 4.13, 4.14, 4.15, 4.16 .

Figure 4.13: The effect of humidity control on drying at 0, 30, 50, 70, 90% ($P^{\circ}_{H_2O}$ = 90°C)

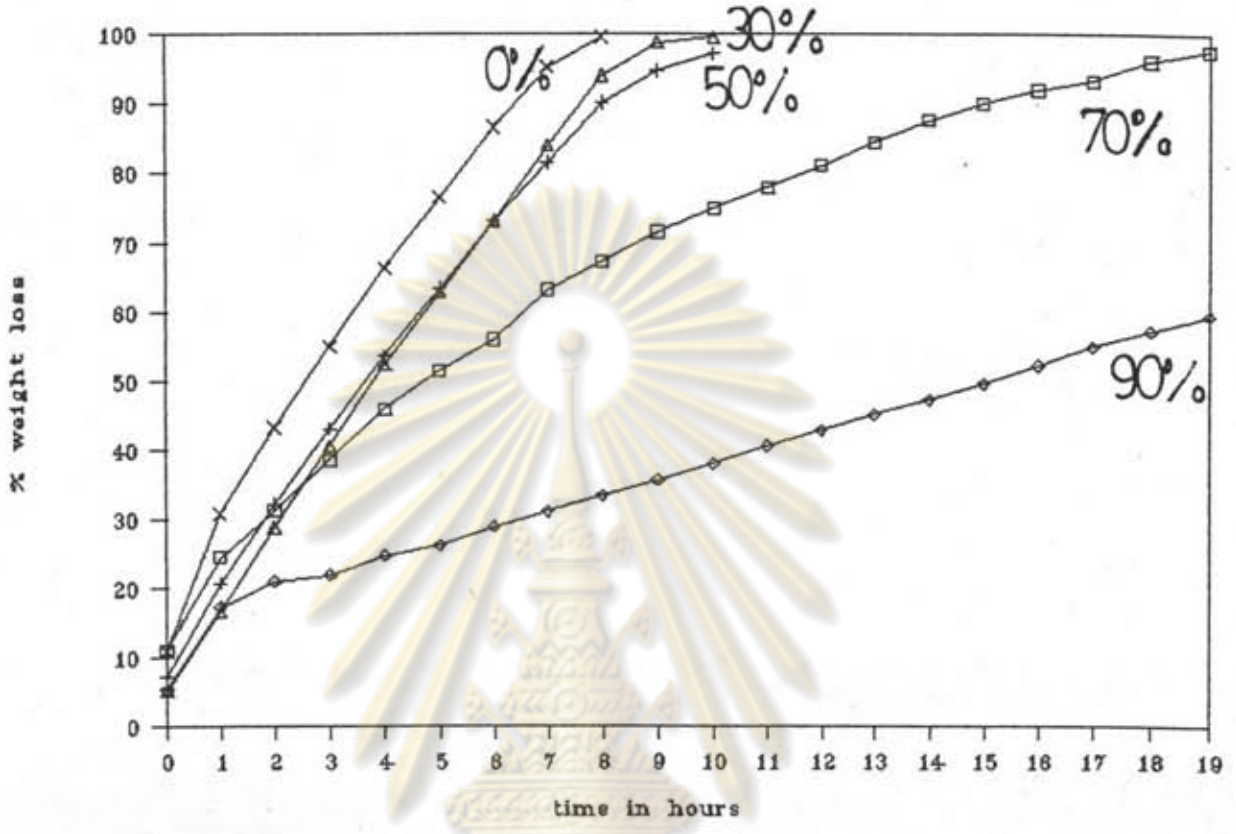

Figure 4.14: The effect of humidity control on shrinking at 0, 30, 50, 70, 90% ($P^{\circ}_{H_2O}$ = 90°C)

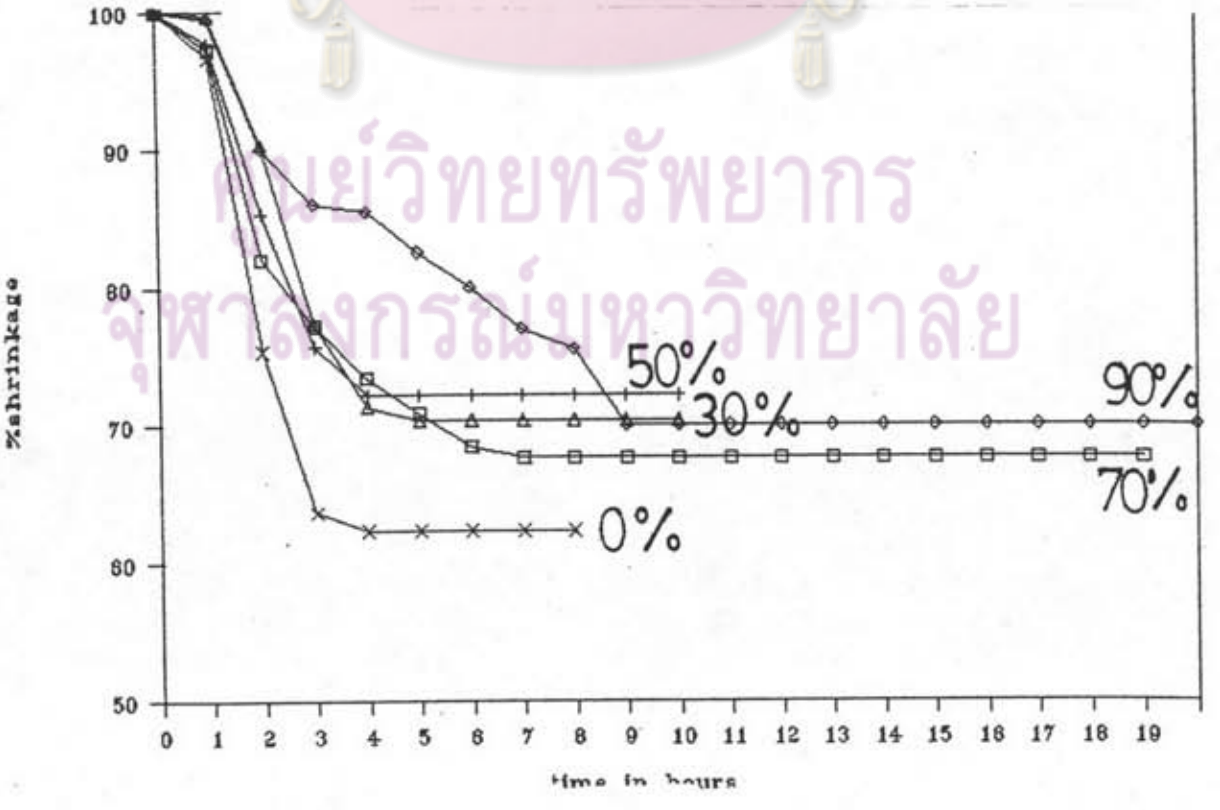

Figure 4.15: The effect of humidity control on weight loss at 0, 30, 50, 70, 90%($P^{\circ}_{H_2O}$ = 70°)

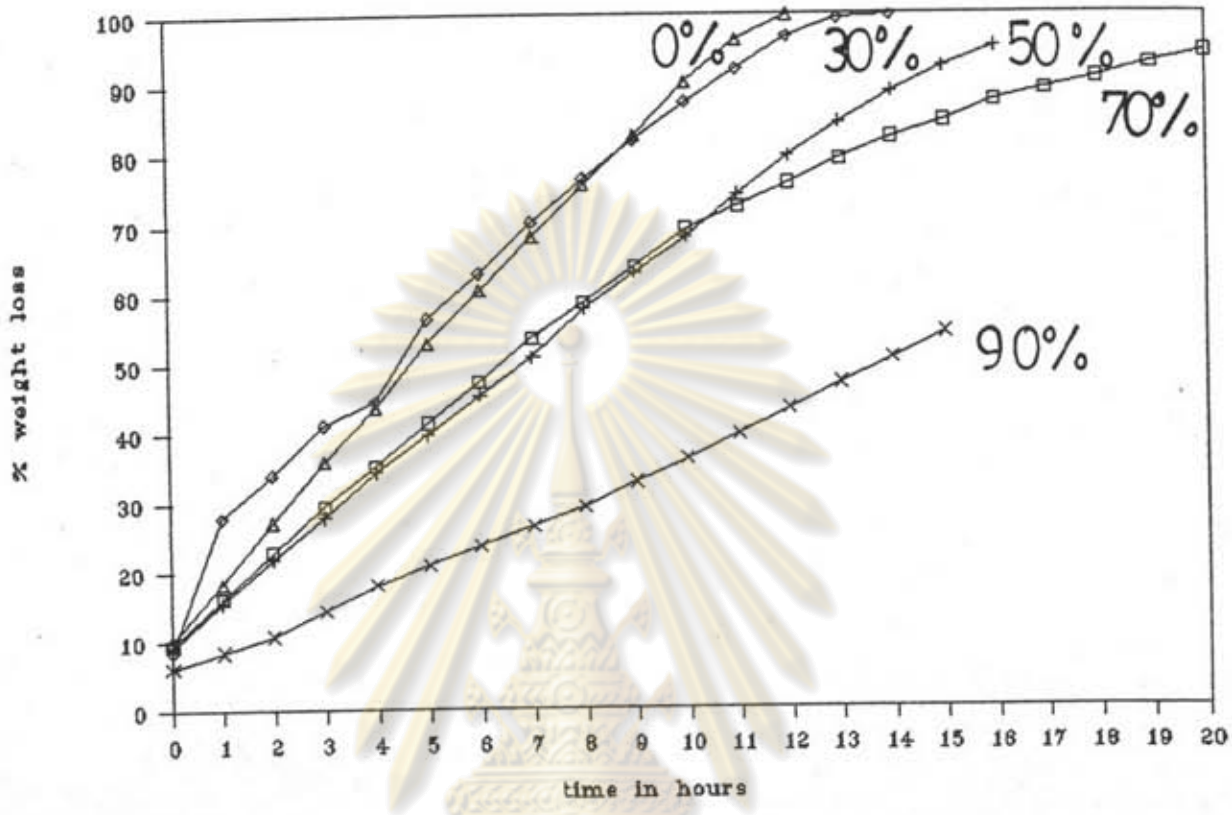

Figure 4.16: The effect of humidity control on shrinking at 0, 30, 50, 70, 90% ($P^{\circ}_{H_2O}$ = 70°C)

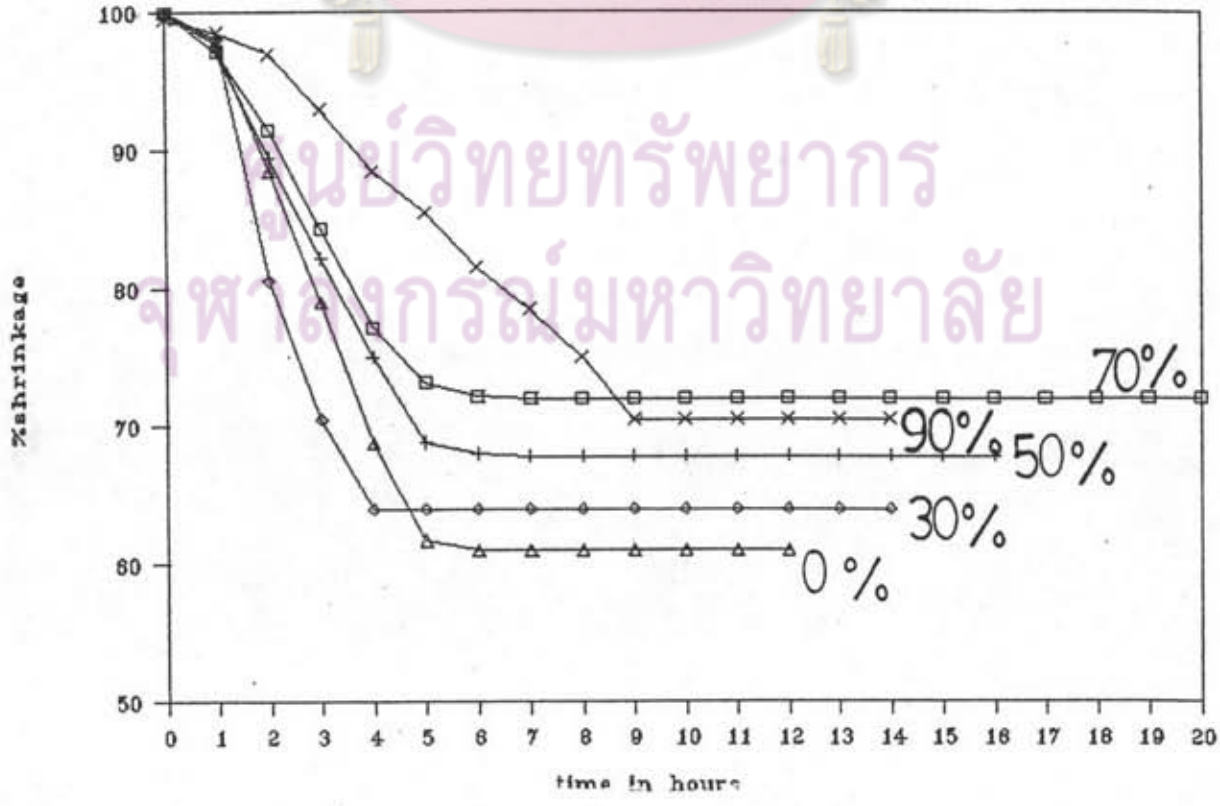

Table 4.5: Relation between water partial pressure and drying rate

P_{H_2O} (mm. Hg)	$P^{\circ}_{H_2O}$ = 70°C		$P^{\circ}_{H_2O}$ = 90°C	
	drying rate	shrinkage rate	drying rate	shrinkage rate
23.37	3.00	-3.71		
52.60	5.04	-5.59	2.37	-2.55
70.11	6.26	-6.72	3.04	-3.15
116.85	5.79	-7.38	4.82	-4.74
157.70	7.60	-9.63	6.37	-6.14
163.59	7.86	-9.95	6.58	-6.41
201.90	8.04	-9.65	6.88	-8.18
262.90			10.17	-11.00
367.96			11.13	-9.80
493.94			11.13	-11.47

R Squared of drying rate is 0.999998 by Lotus program.

R Squared of shrinkage rate is 0.978453 by Lotus program.

Relation between water partial pressure with log slope of drying rate showing in figure 4.17.

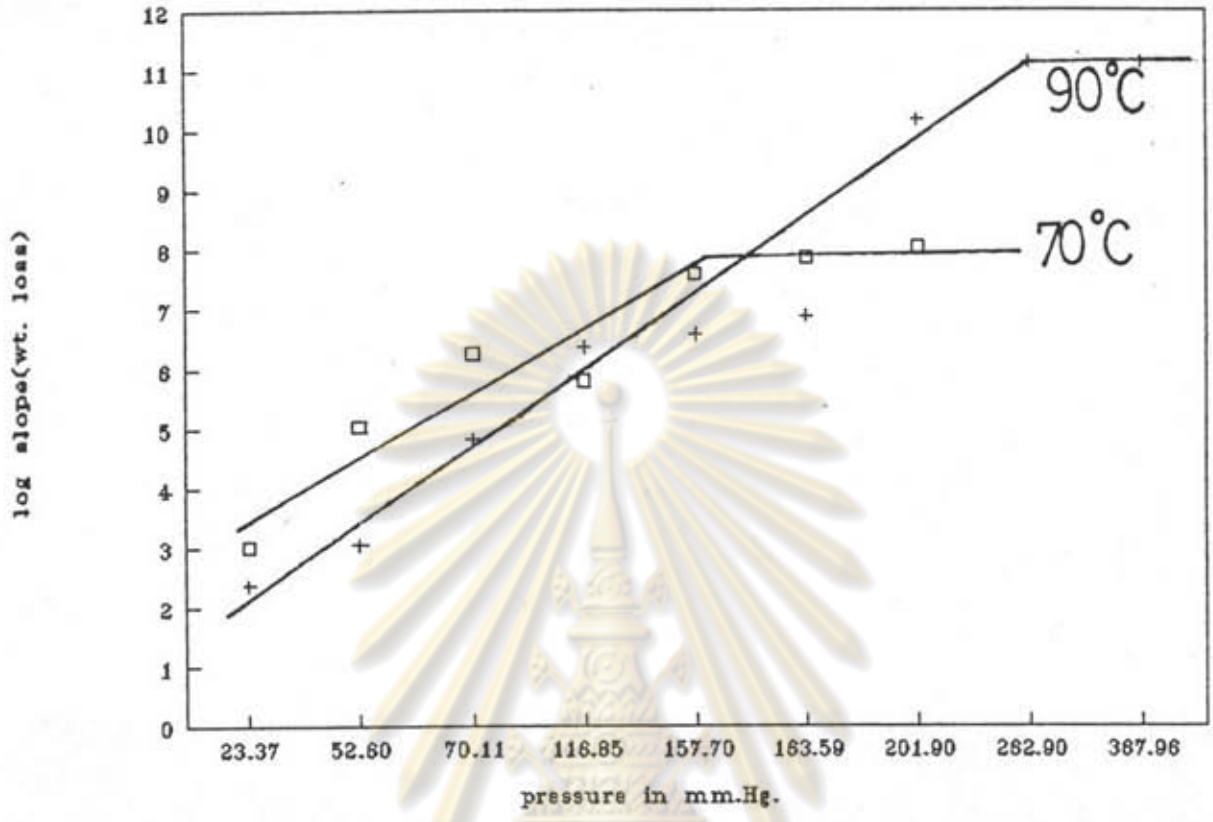

Figure 4.17: Relationship between drying rate and water partial pressure at two selected temperatures

Table 4.6: The effect of time on sintering of OX-50 at 1250°C

time (min)	log time	weight (g.)	density (g/cm^3)	avg density	%shrinkage	avg shrinkage	XRD peak height
10	1.00	0.5065	2.18	2.19	70.93	71.05	0.00
		0.4506	2.20		71.17		
30	1.48	0.5120	2.20	2.21	63.70	71.45	0.00
		0.4532	2.19		78.55		
		0.5335	2.21		71.39		
		0.5541	2.20		71.59		
		0.5448	2.23		72.01		
60	1.78	0.4771	2.20	2.20	70.49	71.32	
		0.5812	2.20		71.77		
		0.5568	2.21		71.43		2.30
		0.5237	2.20		71.43		3.35
		0.6261	2.19		71.47		
90	1.95	0.4695	2.16	2.16	72.20	71.86	
		0.4374	2.20		70.90		
		0.5847	2.20		71.17		2.40
		0.5329	2.09		73.35		
		0.5519	2.14		71.69		2.40
120	2.08	0.5205	2.20	2.20	71.33	71.34	
		0.4977	2.18		72.96		
		0.4966	2.20		70.75		
		0.5521	2.21		70.35		3.25
		0.5179	2.20		71.33		6.05

150	2.18	0.4495	2.18	2.18	71.92	71.41	
		0.4549	2.12		70.42		
		0.5911	2.20		71.43		4.10
		0.4986	2.20		71.83		
		0.5007	2.20		71.43		2.60
180	2.26	0.4420	2.15	2.16	71.93	71.59	
		0.4520	2.12		71.23		
		0.5816	2.17		66.98		
		0.4811	2.17		73.81		
		0.5154	2.20		74.01		2.75
210	2.32	0.4760	2.17	2.14	69.97	71.26	7.05
		0.4426	2.16		71.76		
		0.5014	2.16		71.91		
		0.4696	2.15		72.22		
		0.5955	2.08		70.45		23.40
240	2.38	0.4351	2.11	2.10	72.00	70.96	
		0.4977	2.11		71.58		
		0.6137	2.18		70.64		1.60
		0.6008	2.01		69.60		
270	2.43	0.4770	2.14	2.13	70.80	71.14	10.65
		0.4497	2.14		71.18		
		0.5356	2.10		71.38		
300	2.48	0.4813	2.12	2.12	71.18	70.93	
		0.4409	2.12		70.67		
330	2.52	0.4873	2.11	2.11	71.23	71.24	
		0.5131	2.11		71.24		
360	2.56	0.4424	2.04	2.04	66.08	70.92	
		0.4329	2.03		75.76		

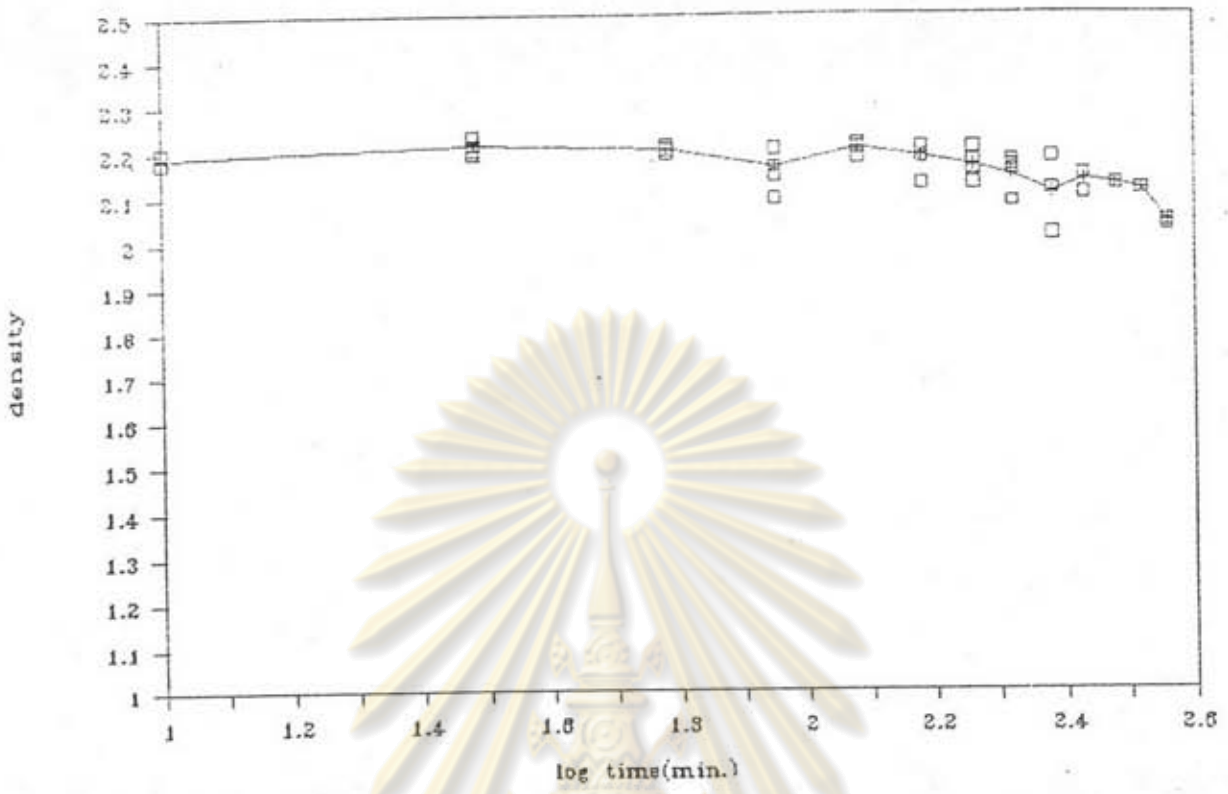

Figure 4.18: Density after sintering at time 1250 °C as a function of time

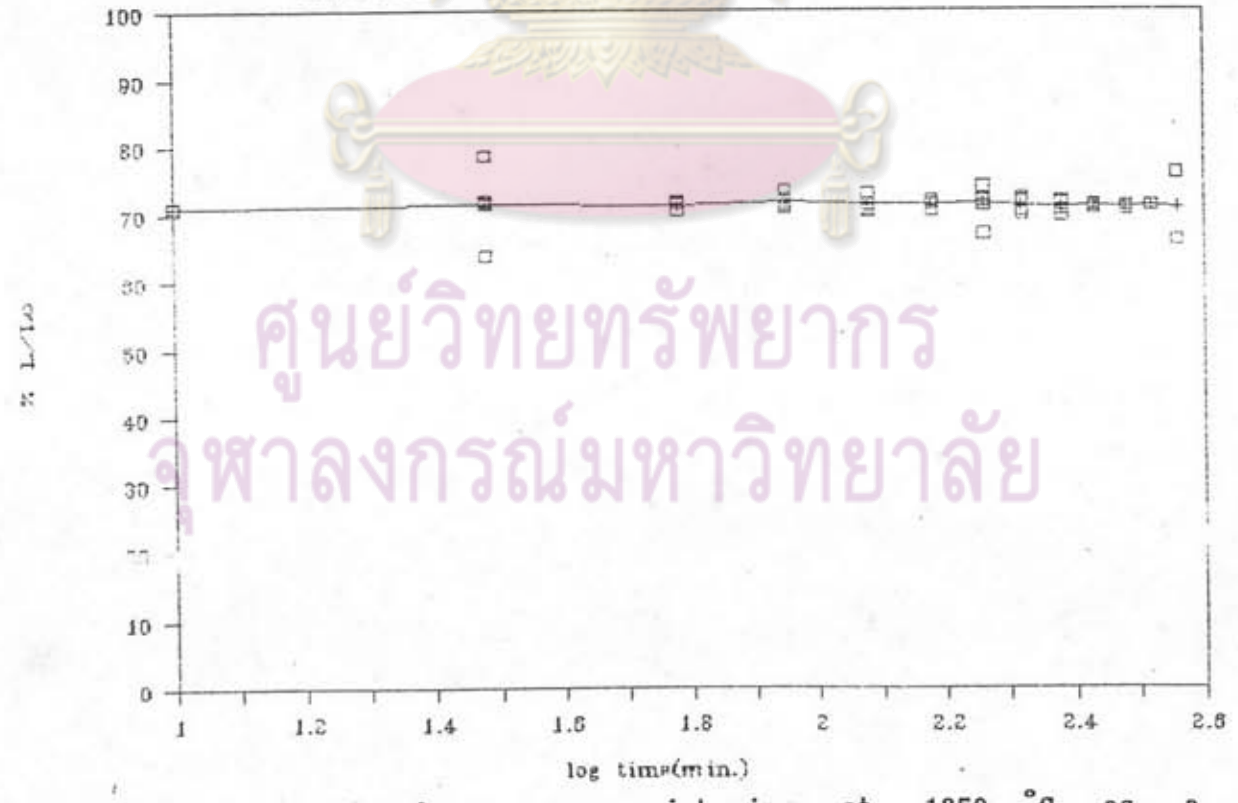

Figure 4.19: Shrinkage upon sintering at 1250 °C as a function of time

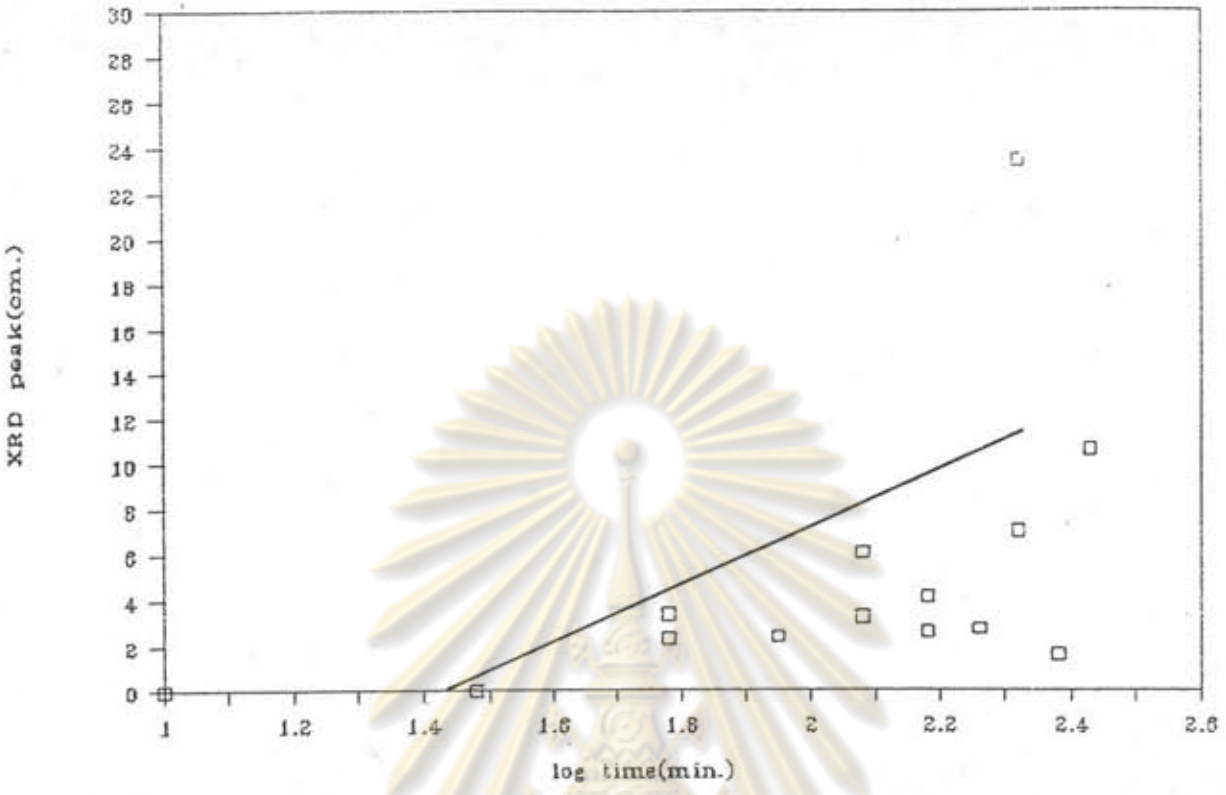

Figure 4.20: Relative XRD peak height at $2\theta = 22^{\circ}$ as a function of time

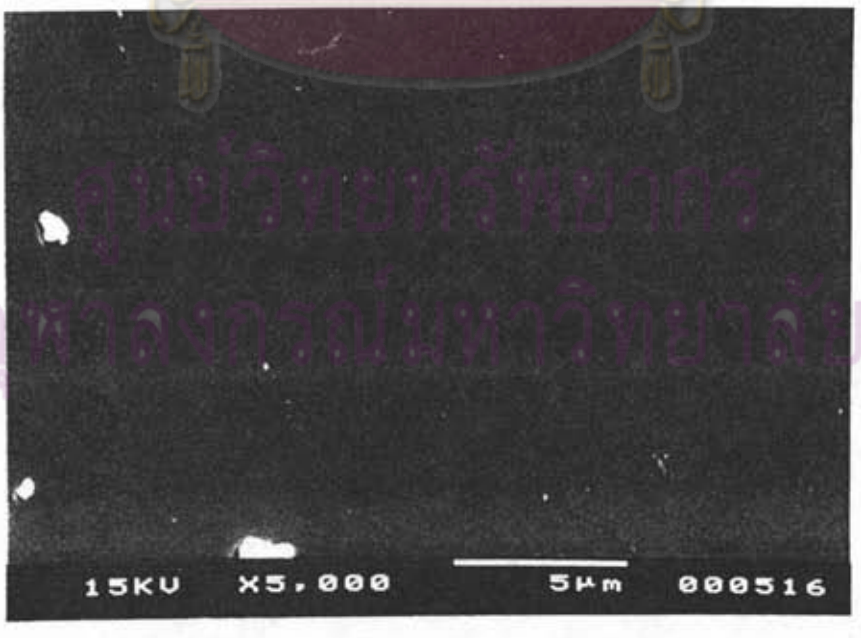

Figure 4.21: SEM micrograph showing of OX-50 (sintered)

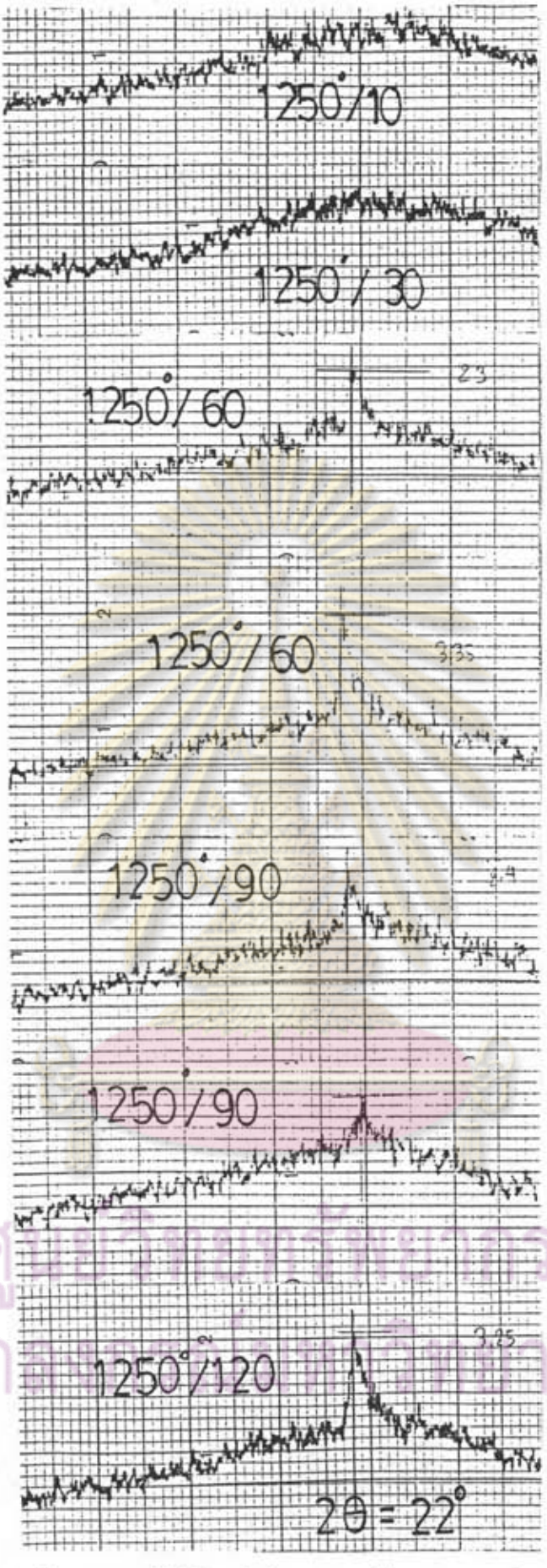

Figure 4.22: X-ray diffraction patterns of OX-50 in the vicinity of $2\theta = 22^{\circ}$ after different sintering times (in min) at 1250 °C

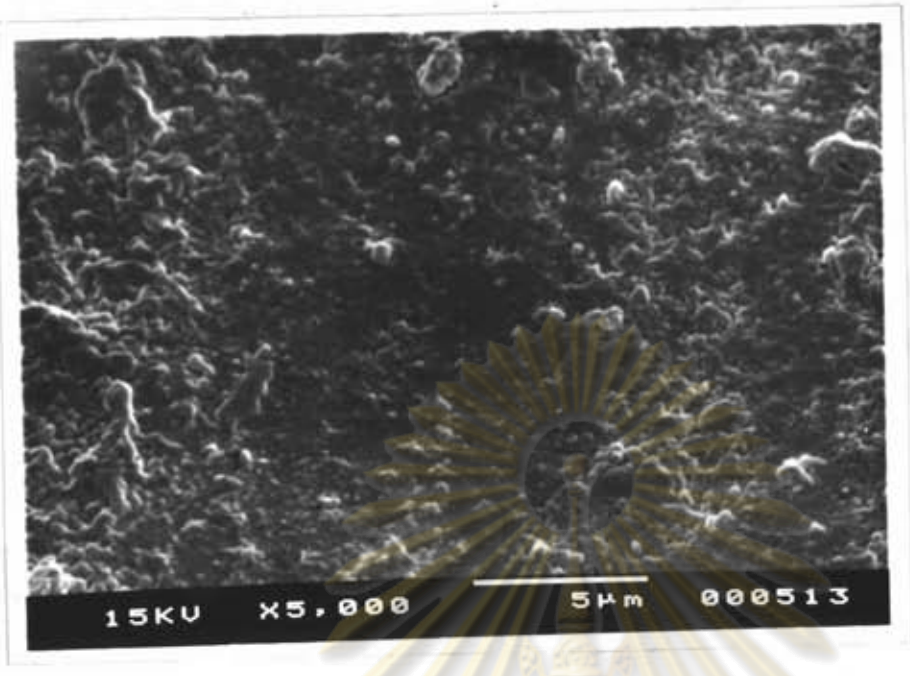

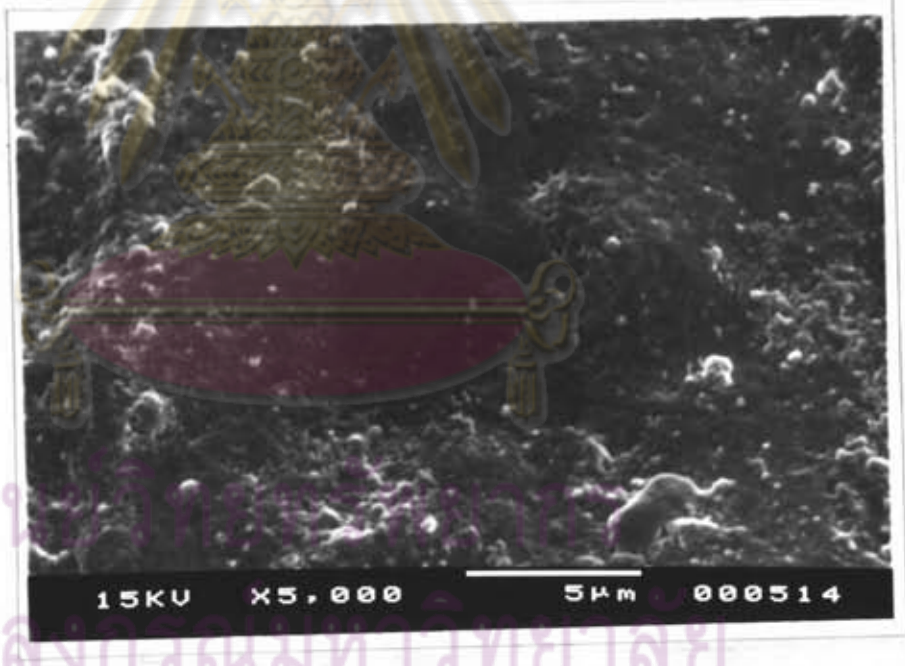

Figure 4.23:SEM micrographs showing heterogeneity of rice husk ash in sintered samples prepared with NH_4F solution (no pH control)

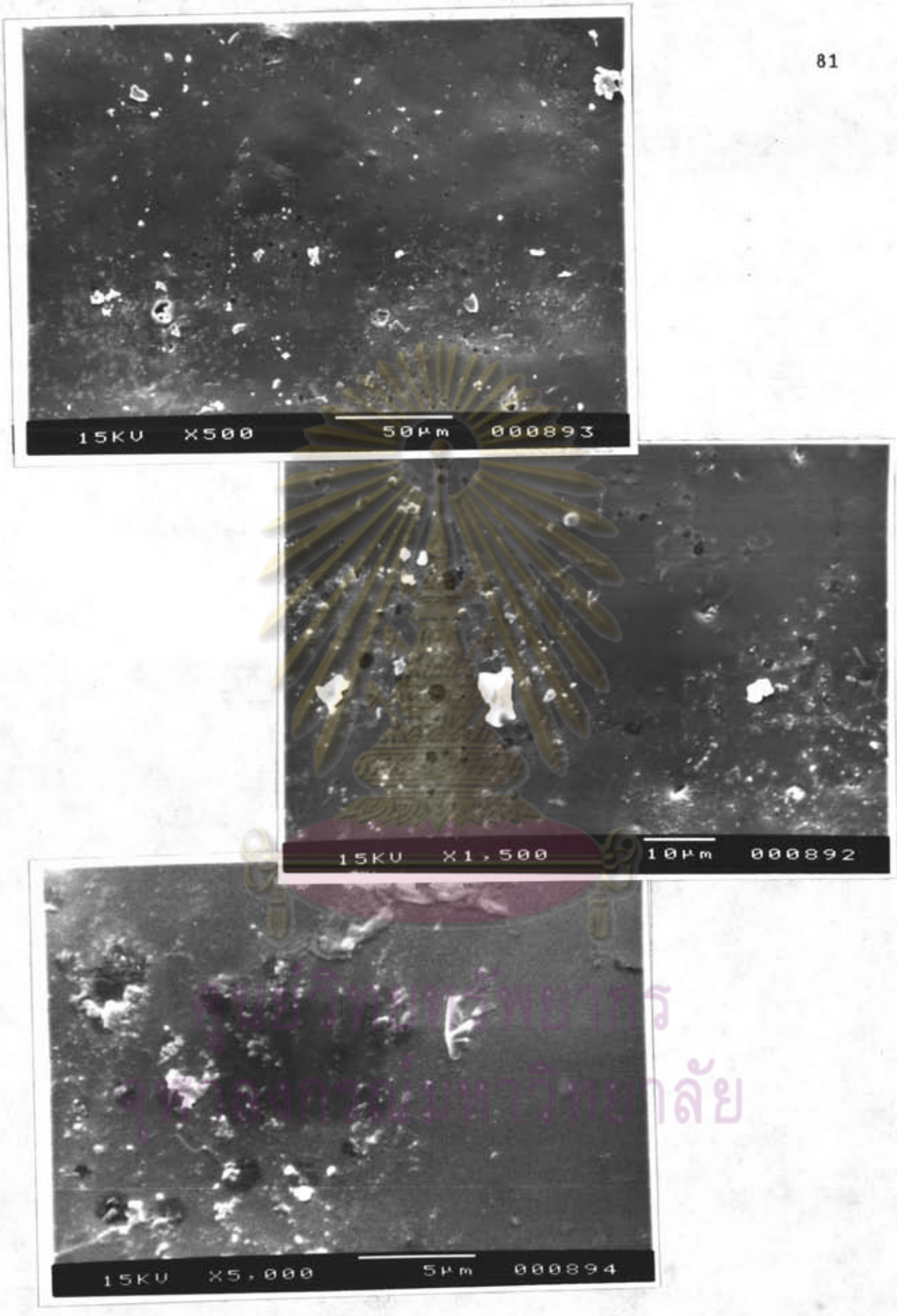

Figure 4.24: SEM micrographs of rice husk ash showing the microstructure after sintering at 1250 °C

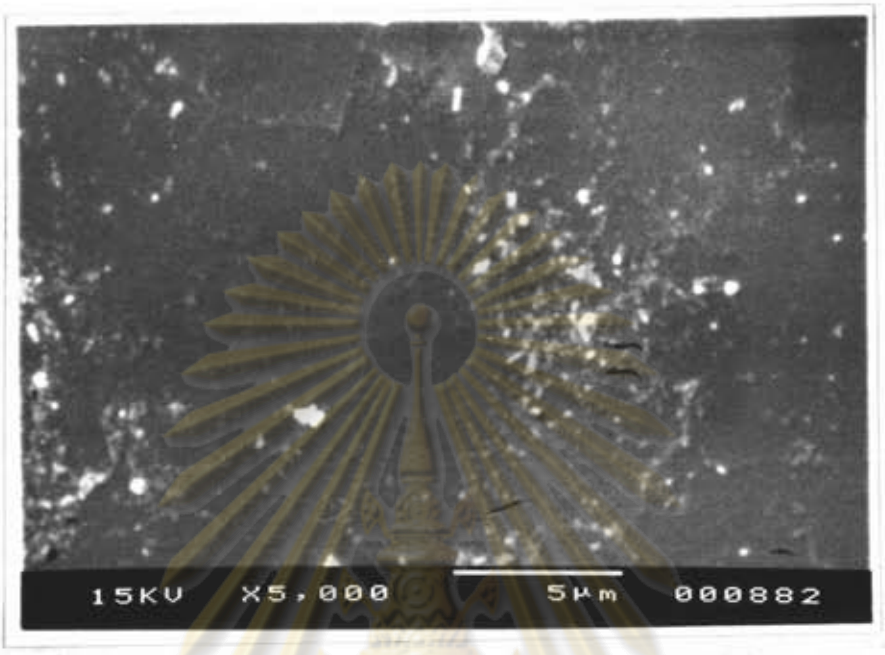

Figure 4.25: SEM micrograph showing the microstructure of rice husk ash after sintering at 1350 °C

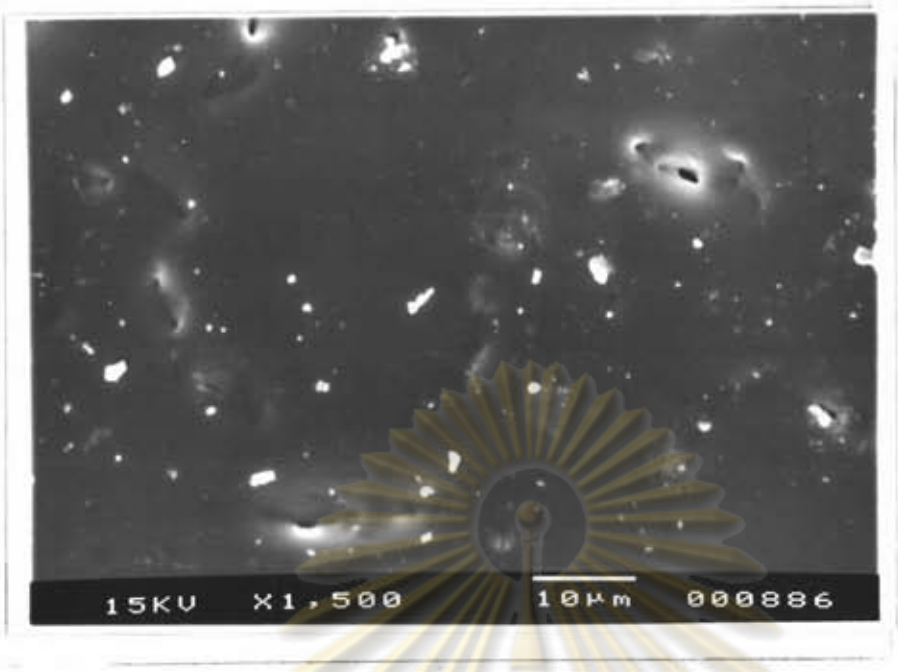

Figure 4.26: SEM micrographs showing the microstructure of rice husk ash after sintering at 1400 °C; surface cracking occures

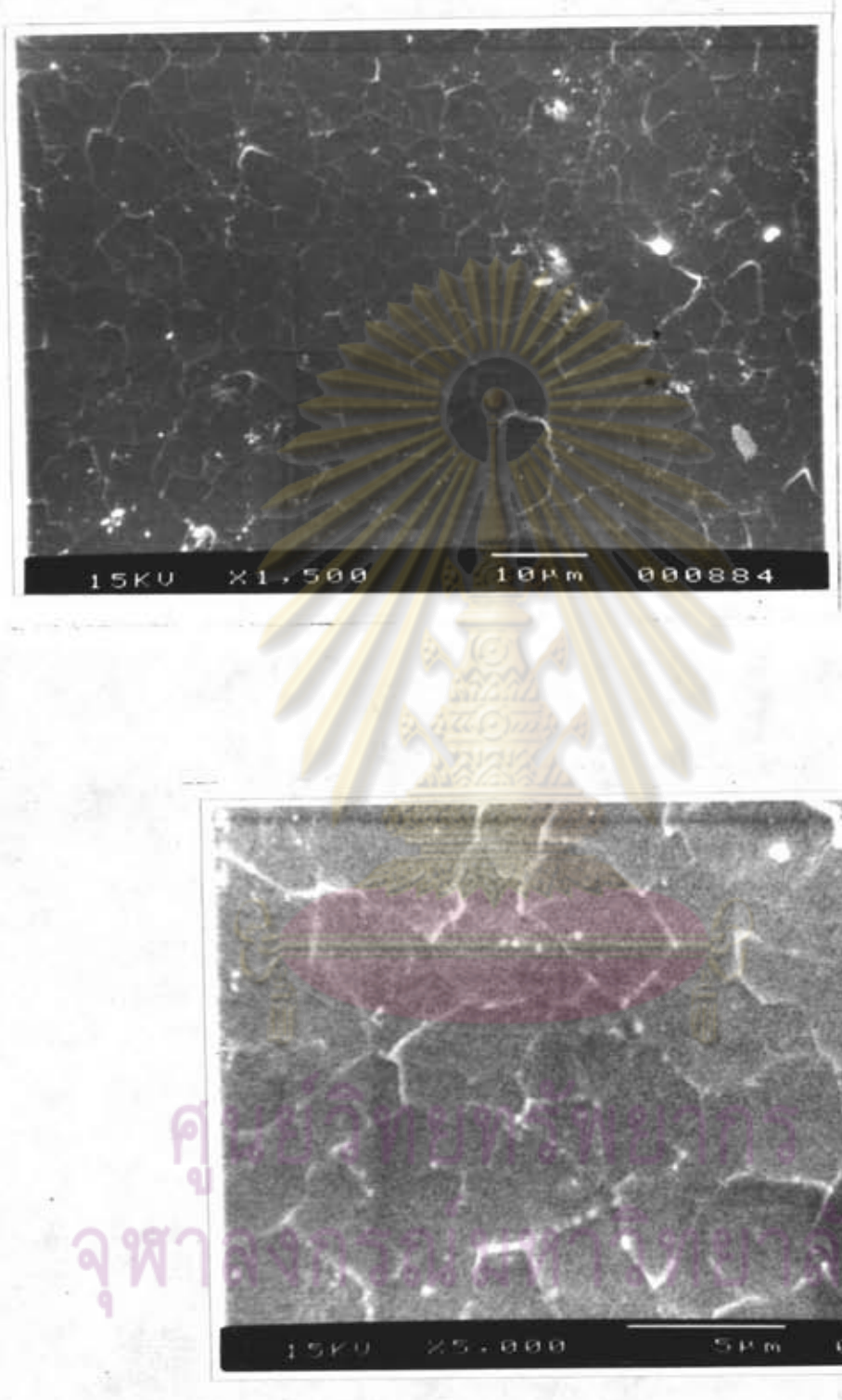

Figure 4.27: SEM micrographs showing microstructure of rice husk ash after sintering at 1450 °C

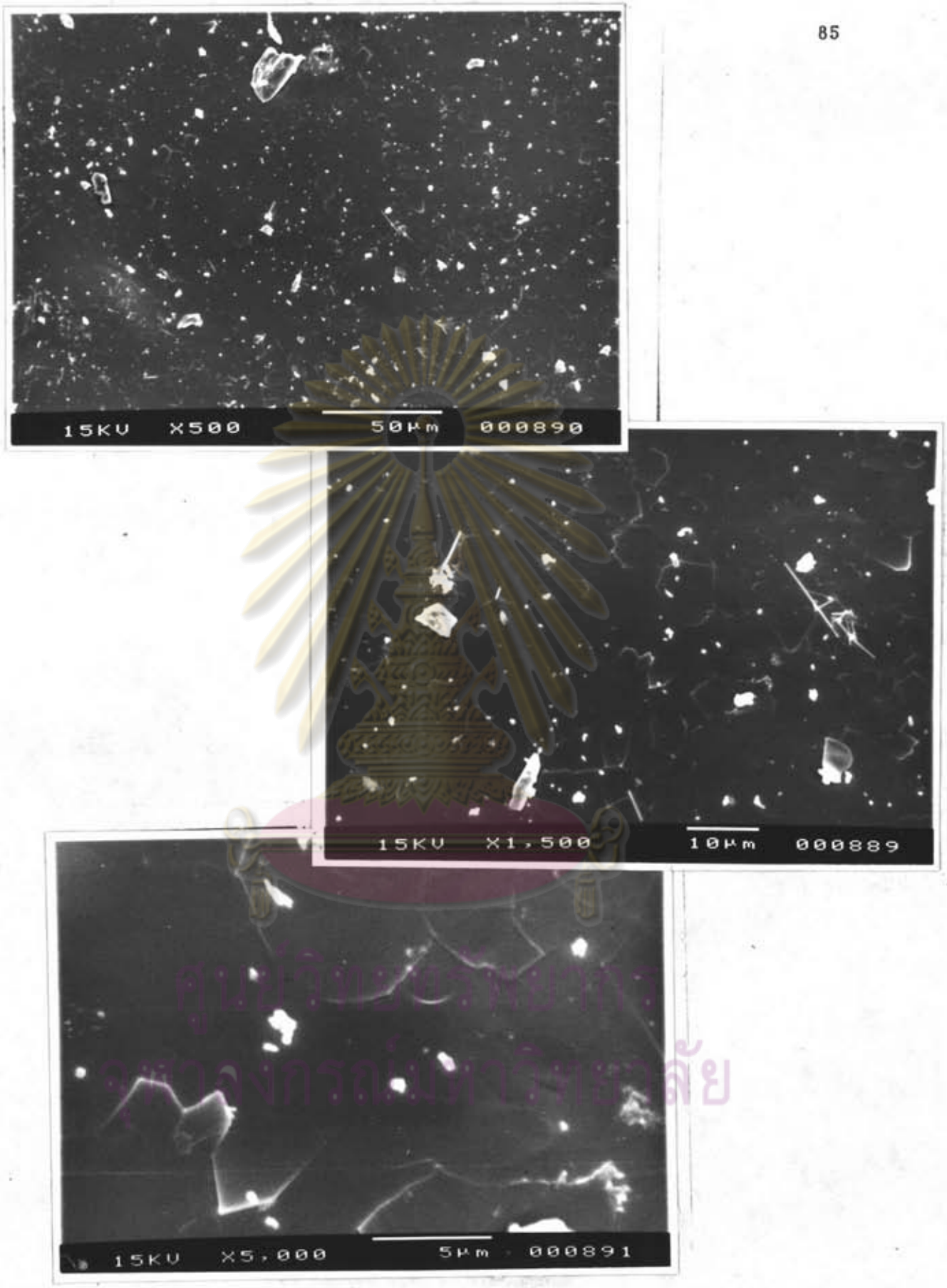

Figure 4.28: SEM micrographs showing the microstructure of rice husk ash after sintering at 1500°C

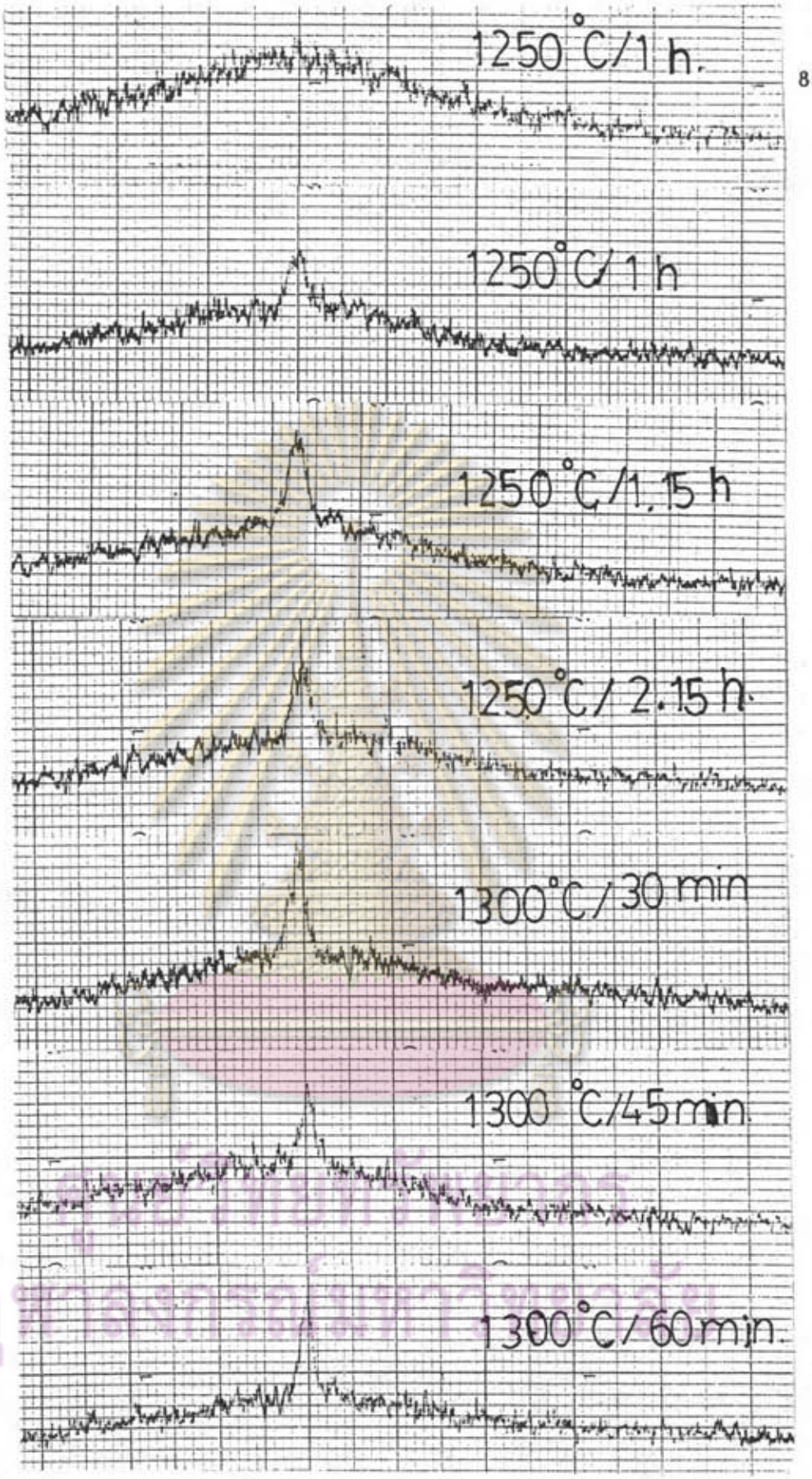

Figure 4.29: X-ray diffraction patterns of rice husk ash showing the effect of temperature and time of sintering; vicinity of $2\theta = 22^{\circ}$

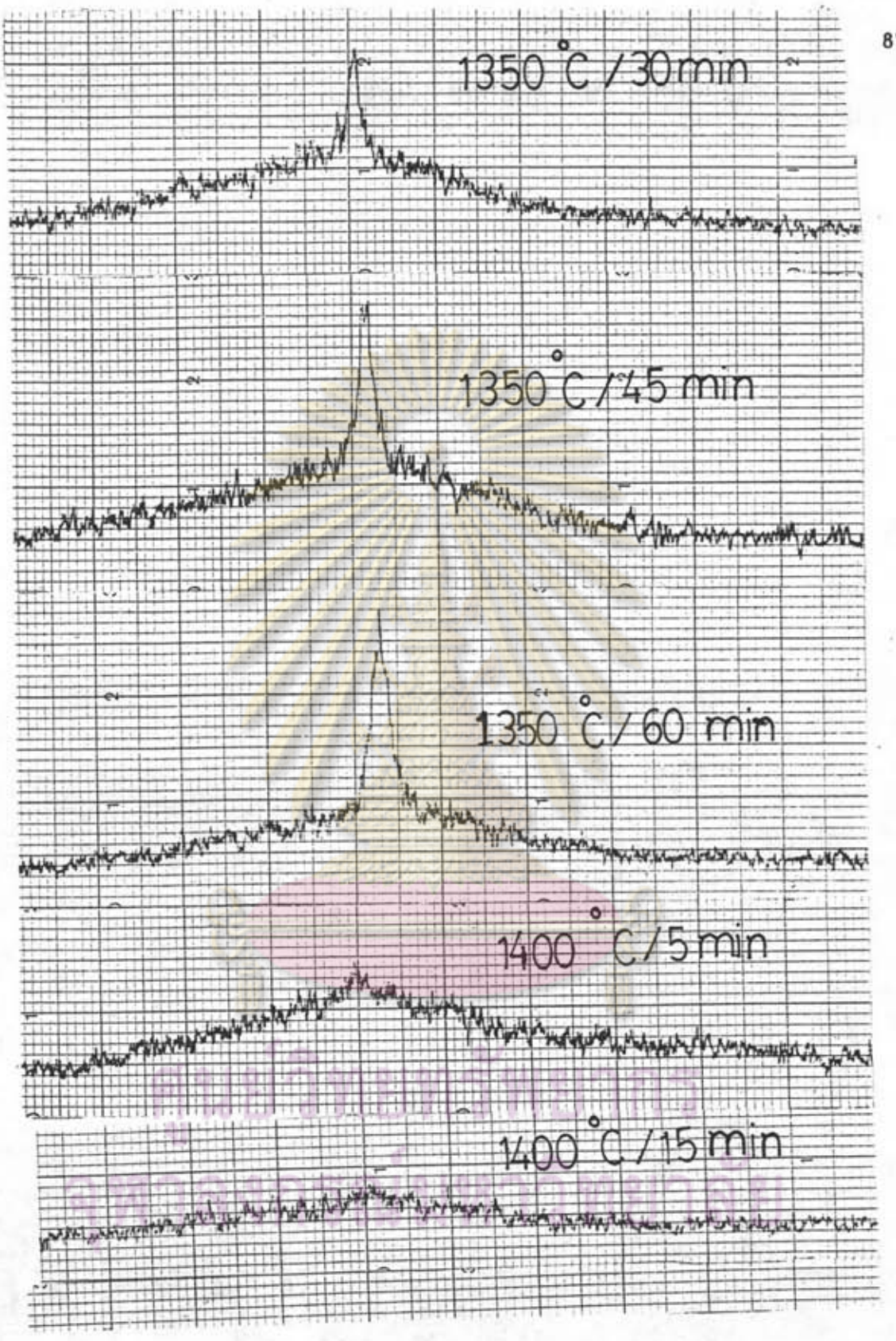

Figure 4.30: X-ray diffraction patterns of rice husk ash showing the effect of temperature and time of sintering; vicinity of $2\theta = 22^{\circ}$

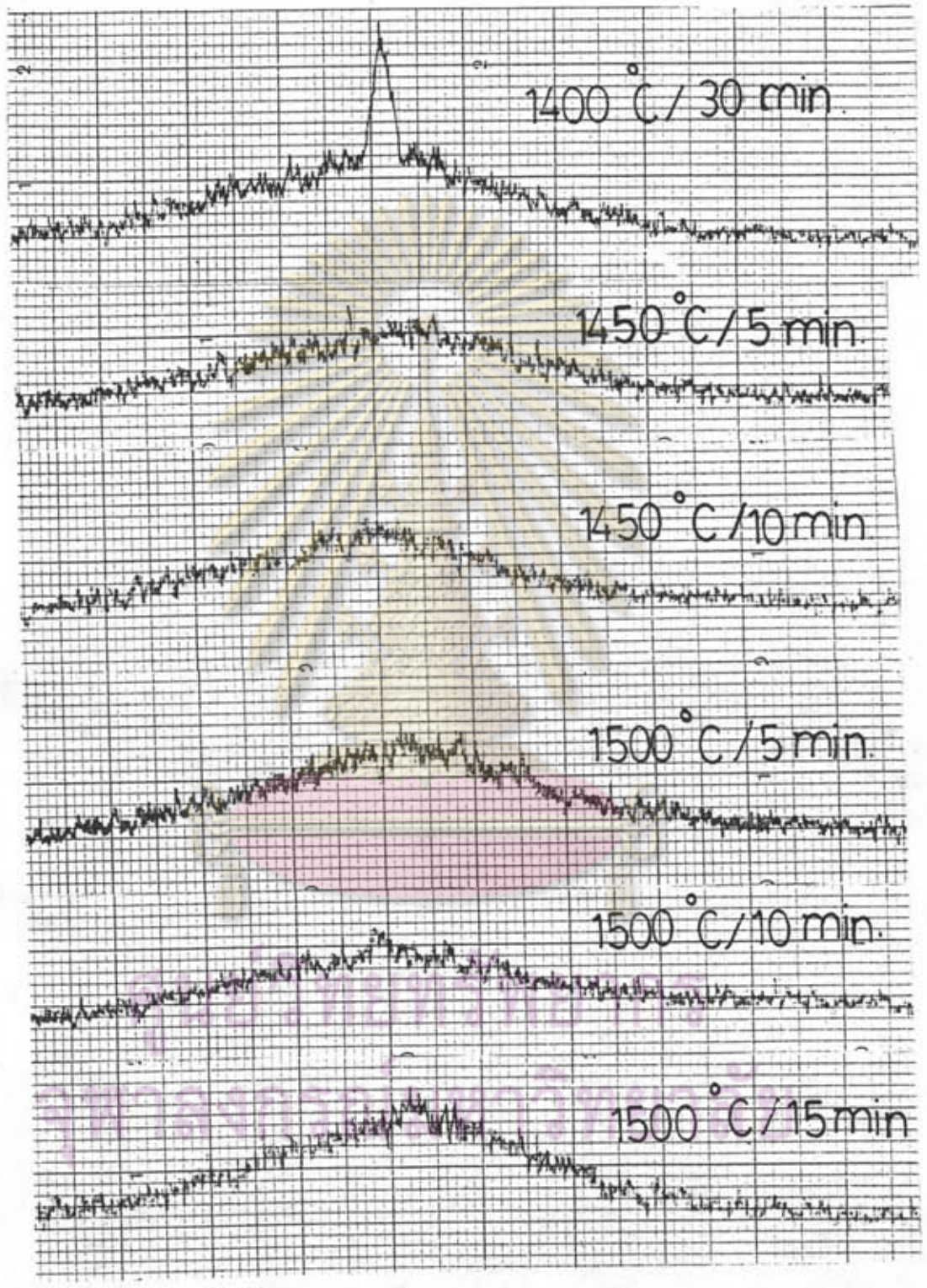

Figure 4.31: X-ray diffraction patterns of rice husk ash showing the effect of temperature and time of sintering; vicinity $2\theta = 22^{\circ}$

Figure 4.32: SiO_2 TTT diagram for rice husk ash and OX-50

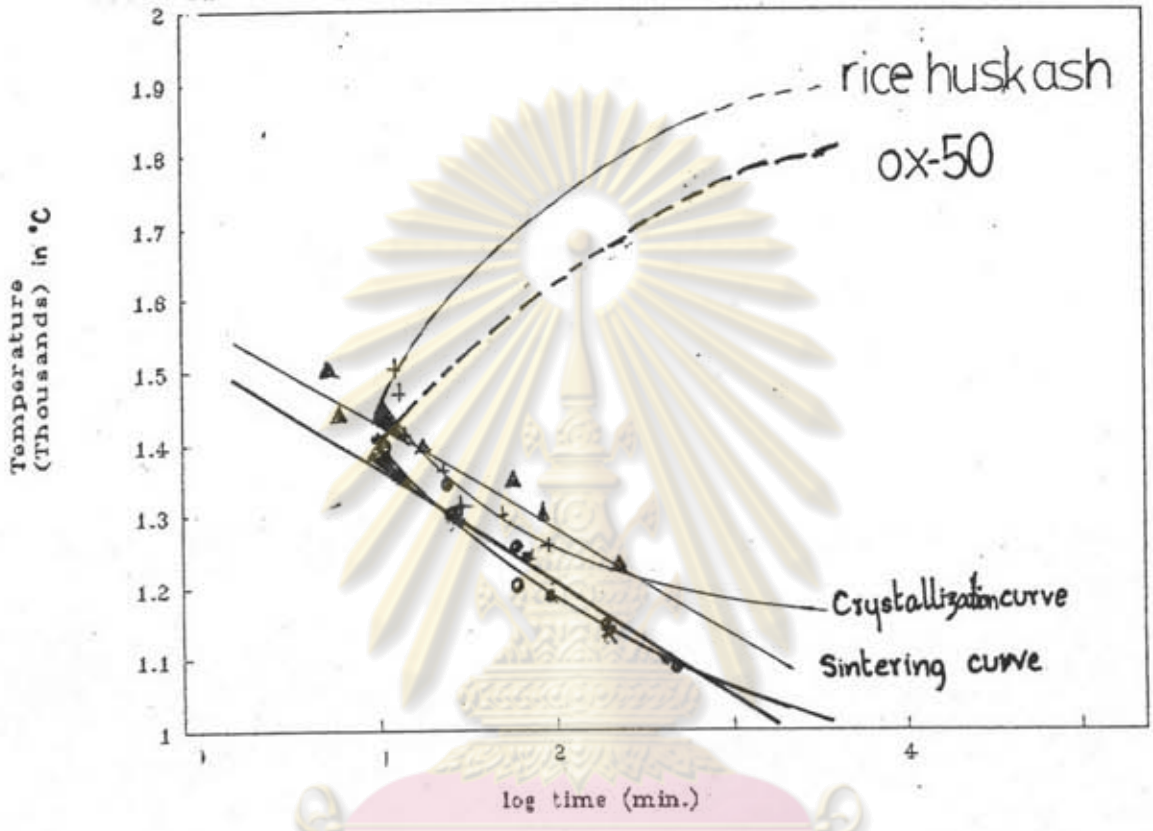

TTT diagrams estimated after the data for densification upon sintering and crystal growth upon sintering for rice husk ash and OX-50.

+ = crystalline curve of rice husk ash

Δ = sintering curve of rice husk ash

* = crystalline curve of OX-50

o = sintering curve of OX-50

Theoritical density of amorphous SiO_2 is 2.20 g/cm^3.

Table 4.7: Results of density (g/cm^3), water absorption, porosity after sintering of rice husk ash gel

Temp.(°C) time(min)	1250	1300	1350	1400	1450	1500
5				2.13 0.25 0.54	2.15 0.19 0.40	2.12 0.11 0.23
10				2.10 0.05 0.11	2.10 0.16 0.34	2.02 0.37 0.71
15				1.91 0.46 0.87		1.99 0.19 0.37
30		2.09 0.45 0.95	2.13 0.11 0.22			
45		2.15 0.10 0.21	2.16 0.05 0.11			
60	2.04 1.40 2.84	2.05 0.34 0.70				

Temp.(°C) time(min)	1250	1300	1350	1400	1450	1500
75	2.04 1.19 2.42					
135	1.92 6.18 11.88					

Table 4.8: Properties of SiO_2 modifications

modification	lattice type	Si-O (°A)	density(g/cm^3)	linear thermal expansion 10^{-6} K^{-1}
low quartz	trigonal	1.61	2.651	12.3
high quartz	hexagonal	1.62	-	-
low cristobalite	tetragonal	1.60-1.61	2.33	10.3
high cristobalite	cubic	1.58-1.69	-	-
low tridimite	monoclinic	1.54-1.71	2.27	21.0
high tridimite	hexagonal	1.53-1.55	-	-
vitreous silica	none	~1.6	2.20	~ 0.5 *)

*) depending on OH content and pore volume

Fig. 4.33 : Dilatogram of sintered silicas